AEDC-TDR-63-21

THE SHOCK SHAPE AND SHOCK DETACHMENT DISTANCE FOR SPHERES AND FLAT-FACED BODIES IN LOW-DENSITY, HYPERVELOCITY, ARGON FLOW

By

A. B. Bailey and W. H. Sims

von Kármán Gas Dynamics Facility
ARO, Inc.

TECHNICAL DOCUMENTARY REPORT NO. AEDC-TDR-63-21

February 1963

AFSC Program Area 750A, Project 8953, Task 895306

(Prepared under Contract No. AF 40(600)-1000 by ARO, Inc., contract operator of AEDC, Arnold Air Force Station, Tenn.)

ARNOLD ENGINEERING DEVELOPMENT CENTER

AIR FORCE SYSTEMS COMMAND

UNITED STATES AIR FORCE

NOTICES

THE SHOCK SHAPE AND SHOCK DETACHMENT DISTANCE FOR SPHERES AND FLAT-FACED BODIES IN LOW-DENSITY, HYPERVELOCITY, ARGON FLOW

By

A. B. Bailey and W. H. Sims

von Kármán Gas Dynamics Facility

ARO, Inc.

a subsidiary of Sverdrup and Parcel, Inc.

February 1963

ARO Project No. VL2159

FOREWORD

The authors wish to acknowledge the assistance of R. Parrish, E. Pinion, and H. Ramm in the interpretation of the photographs and the suggestions of J. Leith Potter in analyzing the results.

ABSTRACT

An experimental investigation has been made to determine the pressure distribution, shock shape, and shock detachment distance for spheres and the latter two characteristics for flat-faced bodies in a heated argon flow where M_∞ = 4 to 14, T_o = 1900 to 4100°K, and Re_2 = 25 to 225.

The modified Newtonian approximation for the pressure distribution, which is strictly an empirical relationship, gives good results when applied to the first 60 deg of a hemisphere under conditions where the body boundary layer and the shock layer merge.

The natural flow visualization produced as a result of the high total temperature and consequent excitation of the argon enabled this study to be made. Photographs taken of the shocks generated by a series of spheres and flat-faced bodies were analyzed with a photo-densitometer to determine the shock shape and shock detachment distance. The blast analogy predicts a difference in the shape of shocks in argon and air at high Mach numbers and Reynolds numbers. An empirical relationship proposed by Love was used to calculate the shock shape in air for Mach numbers corresponding to those of the present investigation.

When this shape was compared to the shape measured in argon at the same Mach number, it was found that the difference in shape was in agreement with that predicted by the blast analogy, i.e., for a constant value of x/D then $(y/D)_{argon}/(y/D)_{air} = 1.16$. Also, it appears even for the lowest Reynolds number tested that nondimensionalized shock shape is independent of Reynolds number for spheres and flat-faced bodies when the effect of Reynolds number on detachment distance is taken into account.

A study of the shock detachment distance indicates that the boundary and shock layers were either incipiently or fully merged in these experiments. Furthermore, for the Reynolds number range of the present tests, the detachment distance is a function of wall temperature, Reynolds number, Mach number, and body shape. As the Reynolds number decreases, the shock detachment distance increases to values more than double the "inviscid" values. Also, for the water-cooled bodies, there is evidence to confirm the decrease in detachment distance to less than the inviscid value, as predicted by Ho and Probstein, before the increase as mentioned above for the lowest Reynolds numbers.

PUBLICATION REVIEW

This report has been reviewed and publication is approved.

Donald R. Eastman, Jr.
DCS/Research

Jean A. Jack
Colonel, USAF
DCS/Test

ARNOLD ENGINEERING DEVELOPMENT CENTER
AIR FORCE SYSTEMS COMMAND
UNITED STATES AIR FORCE
ARNOLD AIR FORCE STATION, TENNESSEE

TRANSMITTAL NOTE

1. The attached report is forwarded for your information and retention.

2. Inquiries relative to any feature of this report should be addressed to this Headquarters, ATTN: AETI.

FOR THE COMMANDER:

John W. McCurdy

JOHN W. McCURDY
LTCOL, USAF
Asst. DCS/Test

CONTENTS

TABLE

ILLUSTRATIONS

NOMENCLATURE

A, a, and n	Constants in Eq. (6)
C_D	Nose drag coefficient
C_p	Pressure coefficient = $\frac{2(p - p_\infty)}{\rho_\infty U_\infty^2}$
D	Body diameter
δ	Shock-wave thickness
J_o	Blast analogy constant, Eq. (7)
K	Factor, Eq. (1)
k	Factor, Eq. (5)
M_2	Mach number immediately behind a normal shock
M_∞	Free-stream Mach number
$\dot{m}$	Mass flow rate
p	Pressure
p_2	Pressure immediately downstream of a normal shock
p_∞	Free-stream pressure
p_q	Impact pressure
p_{o_c}	Reservoir pressure - cold flow
p_{o_h}	Reservoir pressure - hot flow
R_b	Body radius (= nose radius of curvature for sphere)
Re_2	Reynolds number based on body diameter and condition immediately downstream of a normal shock. For purposes of calculating Re_2 this shock is assumed to be unaffected by the boundary layer.
S	Molecular speed ratio
T_o	Reservoir temperature of gas
T_{o_c}	Reservoir temperature of gas - cold flow
T_{o_h}	Reservoir temperature of gas - hot flow
T_w	Body wall temperature
V_2	Velocity immediately downstream of a normal shock
U_∞	Free-stream velocity

u_s	Velocity gradient at the stagnation point
x, y	Ordinates with origin at the apex of the shock
x_b, y	Ordinates with origin at the apex of the body
γ	Specific heat ratio
γ_∞	Free-stream specific heat ratio
Δ	Shock detachment distance, distance from the body to the shock leading edge measured along the axis of symmetry
δ	Boundary-layer thickness
δ^*	Boundary-layer displacement thickness
θ	Angle between the local normal to the surface and the direction of the undisturbed free-stream velocity
λ_∞	Free-stream mean free path
μ_w	Coefficient of viscosity based on wall temperature
ρ_2	Density immediately downstream of a normal shock
ρ_∞	Free-stream density
ρ_w	Density at the wall
ω	Exponent in the viscosity-temperature relationship

1.0 INTRODUCTION

The shock detachment distance in front of blunt bodies at high Reynolds numbers has been studied both theoretically and experimentally. Van Dyke (Ref. 1) presents a theoretical analysis for a series of perfect gases having specific heat ratios of 1, 5/3, and 7/5 and a Mach number range from 1.2 to infinity. This analysis for a sphere indicates that the shock detachment distance is primarily a function of the density ratio across the normal shock, the effect of specific heat variation at fixed density ratio is small, and there is no variation with Reynolds number in essentially inviscid flows. In this analysis it is implied that the shock and boundary-layer thicknesses are small compared with the shock detachment distance. At low Reynolds numbers the shock and boundary-layer thicknesses are no longer small compared with shock detachment distance, and at sufficiently low Reynolds numbers the shock and boundary layer will merge. This implies that there must be a Reynolds number below which the shock detachment distance becomes a function of Reynolds number as well as density ratio.

Probstein and Kemp, Hu and Probstein, and Levinsky and Yoshihara (Refs. 2-4) have made theoretical analyses of this problem in the incipient merged layer flow regime. These analyses have one thing in common: as the Reynolds number is reduced through this regime and the fully merged regime is approached, the shock detachment distance ultimately increases. Reference 2 is based on a constant density assumption for the shock layer, Ref. 3 extends this to consideration of variable density, and Ref. 4 assumes constant density but differs from Ref. 2 in that a monatomic gas (argon) is considered.

The Low-Density, Hypervelocity (LDH) Wind Tunnel, when operated with argon as the working gas, is well suited for low Reynolds number, shock detachment distance investigations. When this tunnel is operated using argon, there is a natural flow visualization thought to be caused by radiation from relaxing metastable argon atoms. This natural glow enables the shock shapes in front of bodies to be seen and photographed. Moulic (Ref. 5) has photographed some shock shapes in a low-density, supersonic wind tunnel at Berkeley. The flow visualization in that case was artifically produced by introducing some nitric oxide and atomic oxygen into the airstream.

Manuscript released by authors January 1963.

Also of interest is the form of the shock wave in front of bodies in low-density flows. There is a considerable amount of data for air at high Reynolds numbers but very little for other gases and very little in any case for low Reynolds numbers. The form of the shock wave is predicted reasonably well by the blast analogy (Ref. 6), and it was believed to be of interest to determine whether that method is still valid in the low-density regime.

For high Reynolds numbers the pressure distribution over a sphere can be calculated reasonably accurately by using the modified Newtonian approximation (Ref. 7). It was believed interesting to ascertain whether this approximation is valid in a flow regime where the shock and boundary layers are merging. A knowledge of the form of the pressure distribution is useful because the stagnation point heat transfer and the growth of the laminar boundary layer are functions of the velocity gradient at the stagnation region which is in turn a function of the pressure distribution.

2.0 APPARATUS

2.1 WIND TUNNEL DESCRIPTION AND PERFORMANCE

The LDH Wind Tunnel is a continuous-type, high-enthalpy wind tunnel in operation at the von Kármán Gas Dynamics Facility (VKF) of the Arnold Engineering Development Center (AEDC), Air Force Systems Command (AFSC), U. S. Air Force. Briefly, the tunnel consists of a d-c arc heater, a stilling chamber, an aerodynamic nozzle, a test chamber with instrumentation, a diffuser, and a pumping system. A schematic drawing identifying some of the components is shown in Fig. 1. A complete description of the LDH tunnel is given in Ref. 8.

In the present tests a number of simple, water-cooled, brass, conical nozzles with a 30-deg total angle were used to accelerate the flow to supersonic speeds. The brass sections have throat diameters of 0.200, 0.397, and 0.750 in. which produce Mach numbers at the exit plane in the range from 4 to 8.5 when argon is the medium. They can be used in conjunction with an aluminum cone frustum extension of 30 deg total angle which continues the expansion of the three basic nozzles to the Mach number range from 7 to 14.

With argon as the working gas the arc heater operates at less than 15 kw. The gas flow rate ranges from 1 to 30 lb/hr, T_o from 1900 to 4100°K, and the reservoir pressure ranges from 1 to 6 psia. At the nozzle

exit and some distance downstream, there is a clearly visible, light blue jet surrounded in most cases by a pink region. On investigation with an impact-pressure probe, the light blue region was found to correspond approximately to the high-speed core of flow. The colors in the flow are thought to be caused by the excitation of argon atoms in a metastable state since the enthalpy is too low for significant ionization. Good in-flow characteristics to the aerodynamic nozzles under test were obtained by using a 3-in.-diam stilling chamber upstream of the nozzle throat, having a length of 4 in. for the 0.200- and 0.397-in.-diam throats and 8 in. for the 0.750-in.-diam throat.

A complete description of the gas flow control, pressure measuring system, reservoir temperature estimate, and rotary probe holder is given in Ref. 9. With regard to the reservoir temperature estimate, the fact that argon is monatomic considerably simplifies this estimate since perfect gas laws apply. Hence, at constant mass flow,

$$T_{o_1} \quad T_{o_2} \left(\frac{p_{o_1}}{p_{o_2}} \right)^{\frac{\gamma}{\gamma}} \quad \text{const.}$$

2.2 TUNNEL OPERATING CONDITIONS

The usable flow regions existing with the aerodynamic nozzles were determined by making impact-pressure surveys. These nozzles were operated in over- and underexpanded states, and for all the flow conditions there was an axial Mach number gradient. It is not considered that the existence of an axial Mach number gradient would measurably affect the flow conditions at the front of a model provided that the front faces of the various models are brought to the same axial station in the flow. Berndt (Ref. 10) has made some estimates as to the effect of conical flow on the measured shock detachment distance for high Reynolds number flows. If it is assumed that there is a similar effect in low Reynolds number flows, then Ref. 10 shows that the present experimental results for shock detachment distance can be in error by as much as 5 percent on this account.

3.0 PROCEDURE

3.1 OPERATING CONDITIONS

The desired nozzle flow was established by adjusting the gas flow rate and arc-heater power input to bring the reservoir conditions to the operating level. When these conditions were achieved, the model under test was brought to a predetermined axial station on the nozzle centerline.

3.2 PHOTOGRAPHIC TECHNIQUE

The camera used in this series of tests was a standard 4 x 5 Speed Graphic with fittings such that a Polaroid back could be attached to it. The camera was mounted outside the tunnel, and the model under test was viewed through one of the windows in the test chamber. A 13-in. focal length lens which could be stopped down to f/5.6 was used with the camera.

The relatively low intensity of the glow presented some problems in defining the film and camera settings that would give the best pictures. It was determined by means of a trial and error procedure that good results could be obtained with Kodalith ASA 2 film. It was found that with the lens stopped down to f/5.6 and by varying the exposure from two to four seconds, dependent on the model position with respect to the nozzle exit plane, good quality negatives could be obtained. A typical photograph is shown in Fig. 2.

3.3 SPHERE PRESSURE MEASUREMENTS

Because of the small size of the model (0.50-in. diam) and the need to have as large an orifice as possible from pressure lag-time considerations, it was not practical to put more than one orifice on a model of this size. Therefore, the pressure distribution over the front face of the sphere was obtained by using a number of models each with one orifice at a different angle to the horizontal axis of the sphere. In all, eight water-cooled models were made with 0.052-in.-diam orifices located at 0, 15, 30, 45, 60, 75, 90, and 100 deg to the horizontal axis. Each of the models was mounted on a sting which could be attached to the tunnel probe carrier. With this arrangement it was possible to mount the models such that the pressure sensing orifices were positioned to within ±1.0 deg of the nominal setting.

For each flow condition the front face of the sphere was brought to the predetermined axial position and the pressure was measured using a Pace transducer with an operating range of ±0.1 psi.

4.0 DISCUSSION OF RESULTS

4.1 SHOCK DETACHMENT DISTANCE

4.1.1 Analysis of Photographs

Because of the low-density flow conditions existing in the present tests, it is no longer valid to assume that the shock wave is a discrete

discontinuity. For example, Levinsky and Yoshihara's (Ref. 4) analysis, in the region of the stagnation point, indicates that at the lower Reynolds numbers the variation in density from the front of the shock to the body is gradual and continuous. If it is assumed that the density of the film negative in this region is proportional to the gas density, then the front of the shock will be determined by the point at which the film density starts to increase.

A photo-densitometer was used to determine the position of the shock leading edge, the front face of the sphere, and, where possible, the back face of the sphere. The shock leading edge was determined for a whole series of off-axis stations. The advantage of this is that it provided the shock shape data required in another part of this work, and also, by drawing a smooth curve through the measured points, errors introduced by random measuring errors in stand-off distance were minimized. This type of error is particularly critical in the determination of the shock detachment distance with the smallest spheres. The position of the photo-densitometer carriage can be determined to 0.001 cm; however, the random measuring error can be as much as ±0.005 cm, which, for the smallest spheres, implies a maximum error of approximately ±10 percent in the shock detachment distance. This is the greater error, and in general the error should be less than this for a negative of good quality.

4.1.2 Sphere Results

Two sets of spheres were studied in this experiment: one set consisted of uncooled, stainless steel, ball bearings with diameters ranging from 0.250 to 0.688 in. and the other set consisted of water-cooled brass spheres with diameters ranging from 0.240 to 0.749 in.

A preliminary study of the effect of wall temperature on the shock detachment distance indicated that the detachment distance was quite sensitive to relatively small changes in wall temperature. Because of this temperature sensitivity, the uncooled models were allowed to reach their equilibrium temperature before a photograph was taken. The time to reach this equilibrium temperature was determined by measuring the sphere temperature with a chromel-alumel thermocouple attached to the rear face of the sphere, at a series of time increments after the sphere was brought into the hot stream. It was found from this investigation that the equilibrium condition was attained in a relatively short time (3 min.) and that the wall temperature was approximately 1000°K. Previous experience with water-cooled probes in the LDH Wind Tunnel has shown that the water-cooled spheres should quickly reach an equilibrium state and that the wall temperature for these cases is approximately 300°K.

In Figs. 3 and 4 the results of the determination of the shock detachment distance for the cooled and uncooled spheres are plotted in the form Δ/R_b vs Re_2. A study of these curves shows the dependence of shock detachment distance on Mach number, Reynolds number, and wall temperature. For the range of Reynolds numbers of the present tests, the shock detachment distance increases with decrease of Reynolds number. This is in qualitative agreement with the theoretical predictions of Refs. 2-4 for the variation of shock detachment distance with Reynolds number in the incipient merged layer regime. Furthermore, it is shown that, for a particular Mach number and Reynolds number, as the wall temperature increases the shock detachment distance increases. This is in qualitative agreement with results of Ref. 4.

It is of interest to consider the relative magnitudes of the shock-layer and laminar boundary-layer thicknesses at the flow condition of the present tests. Ziering, Ek, and Koch (Ref. 11), using the Boltzmann equation, present a solution to the problem of determining the shock-wave thickness. A comparison of experimental data obtained on shock thickness in argon with this theory indicates that it gives a good estimate of the shock-wave thickness. Reference 11 shows that the shock-wave thickness is a function of the free-stream Mach number and mean free path. The form of this relationship for argon is shown in Fig. 5. Since there is no reason to doubt the validity of this relationship at low Reynolds numbers, the shock-wave thickness has been derived from Fig. 5 for the range of flow conditions of the present tests. Some typical values are shown plotted in terms of body radius in Figs. 3 and 4. It can be seen that the calculated shock-wave thickness is always an appreciable percentage of the measured shock detachment distance at these low Reynolds numbers, and in some cases it is shown to be larger than the measured shock detachment distance. This may be attributable to the close proximity of the cooled body and consequent heat transfer through the viscous shock layer. This possibility is not considered in the theory which considers isolated shocks.

The laminar boundary-layer thickness at the stagnation point can be calculated for the "thin" boundary-layer case using data contained in Ref. 12, where it is shown that the laminar boundary-layer displacement thickness at the stagnation point can be written in the following form:

$$\delta^* \sqrt{\frac{u_e \rho_w}{\mu_w}} \left(\frac{T_w}{T_0}\right) \quad K \qquad (1)$$

where K is a factor solely dependent on the ratio of wall to stagnation enthalpy and is given in Ref. 12. If it is assumed that the pressure distribution in the region of the stagnation point is adequately defined by the

modified Newtonian approximation, then the velocity gradient at the stagnation point for a hemisphere can be written in the form:

$$u_s = \frac{1}{R_b}\sqrt{\frac{2}{\rho_2}(p_2 - p_\infty)} \tag{2}$$

when $M_\infty \gtrsim 6.0$, then $p_2 \gg p_\infty$ and Eq. (2) may be rewritten as

$$u_s = \frac{1}{R_b}\sqrt{\frac{2}{\gamma}}\left(\frac{u_2}{M_2}\right) \tag{3}$$

Substituting this value for u_s in Eq. (1), and writing ρ_w and μ_w in terms of ρ_2, M_2, T_2, and T_w, Eq. (1) becomes, for the hemisphere,

$$\frac{\delta^*}{R_b} = K\left(\frac{\gamma}{2}\right)^{1/4}\left(\frac{2M_2}{Re_2}\right)^{1/2}\left(\frac{p_2}{p_o'}\right)^{1/2}\left(\frac{T_o}{T_w}\right)^{\frac{1-\omega}{2}}\left(\frac{T_o}{T_2}\right)^{\frac{1+\omega}{2}} \tag{4}$$

For a constant value of γ the product of the terms containing T_o/T_2, M_2, and p_2/p_o' is very nearly constant for a wide range of free-stream Mach numbers ($5 < M_\infty < 20$). The factor K is a function of the ratio of the wall to stagnation temperature, and K changes from negative to positive as T_w/T_o increases from zero to unity. This means that for highly cooled bodies the displacement thickness in the stagnation region is negative. The magnitude of the displacement thickness is a function of the parameter $\left(T_o/T_w\right)^{\frac{1-\omega}{2}}$.

In the present context it is considered that the boundary-layer thickness, δ, is a more meaningful parameter than δ^*. Reference 12 shows that there is a relationship between δ and δ^* which is a function of wall to stagnation temperature ratio only. Substituting this relationship into Eq. (4) gives

$$\delta/R_b = k\left(\frac{\gamma}{2}\right)^{1/4}\left(\frac{2M_2}{Re_2}\right)^{1/2}\left(\frac{p_2}{p_o'}\right)^{1/2}\left(\frac{T_o}{T_w}\right)^{\frac{1-\omega}{2}}\left(\frac{T_o}{T_2}\right)^{\frac{1+\omega}{2}} \tag{5}$$

where in this case k always has a positive value. Typical values of the boundary-layer thickness have been calculated from Eq. (5) and are plotted in Figs. 3 and 4.

For the same Mach number and Reynolds number, Eq. (5) predicts that as the wall to stagnation temperature ratio increases, the boundary-layer thickness decreases. Equation (4) predicts that for the same conditions as above, the displacement thickness increases with an increase

in wall to stagnation temperature ratio. In considering the case where the shock and boundary layers are merged, it is apparent that the displacement thickness does not lose its significance; but the total thickness probably is more important because it indicates the degree of viscous effect in the shock layer, i.e., the nearness to merging. Naturally, both the calculated shock-wave and boundary-layer thicknesses presented here are not exact under the very low Reynolds number conditions being studied. They are presented only for qualitative comparisons.

If the boundary-layer thickness, as computed by a theory applicable to the case $\delta \ll R_b$, is considered to be a reasonable approximation, then Fig. 3 shows that all of the results of this test are in the fully merged regime. It is of interest to note that the form of the measured shock detachment distance variation with Reynolds number is qualitatively similar to the variation of shock-wave and boundary-layer thickness with Reynolds number.

In the merged-layer cooled model case, the temperature immediately behind the shock is reduced to a value less than the stagnation temperature. In Ref. 11, for example, shock-wave thickness is computed and presented in terms of a ratio of shock thickness to free-stream mean free path. Instead of referencing shock-wave thickness to the free-stream mean free path, one may consider a value of mean free path which is the average of the free stream and that just downstream of the shock wave. If the temperature just downstream of the shock is reduced because of wall cooling, then the average value of the mean free path will be reduced, and hence the shock thickness will also be reduced. This, plus the influence of cooling on density in the shock layer, would have the effect of reducing the rate of increase of shock-layer thickness with decrease of Reynolds number. Some confirmation of this is contained in Figs. 3 and 4 when the data for M 6 are compared. There it will be noted that shock-layer thickness at higher Reynolds numbers is greater for the uncooled body which theoretically has the thinner boundary layer and less cooling of the shock layer.

The fact that, for the highest Reynolds numbers tested here, the uncooled sphere shock detachment distance is greater than that for the cooled spheres may be explained by the fact that in the first case the displacement thickness is small but positive; whereas in the latter case, it is small but negative--the sum of these two values accounting for the difference in measured detachment distance.

A method of correlating the present results with those obtained for other flow conditions is suggested in Ref. 13 where $(\Delta/R_b)/(\Delta/R_b)_{inviscid}$ is plotted against Re_2. Schwartz and Eckerman (Ref. 14) and Vas, et al. (Ref. 15), made some tests to determine the shock detachment distance

in argon and helium, respectively, at high Reynolds numbers, the results of which are shown in Fig. 6. The inviscid values for (Δ/R_b) for the present tests were taken from this curve.

Using the above-mentioned parameter, the present results and the theoretical analyses of Refs. 2-4 are compared in Fig. 7. The qualitative effect of wall cooling on the shock detachment distance as predicted by Levinsky and Yoshihara is confirmed. The decrease of shock detachment distance to a value less than the "inviscid" value, as predicted by Ho and Probstein, is qualitatively confirmed in that some measured values of $(\Delta/R_b)/(\Delta/R_b)_{inviscid}$ are less than unity. The constant-density solution of Probstein and Kemp should approximate more closely to the uncooled model condition than to the cold wall case; Fig. 6 shows this to be true. It is important to remember that the results obtained by Ho and Probstein and Probstein and Kemp apply to air, whereas the present data and the results of Levinsky and Yoshihara apply to argon.

It is considered pertinent here to emphasize that the value Δ quoted herein is the distance from the face of the body to the leading edge of the shock. For high Reynolds numbers the flow in front of a body is divided into three regions: the shock layer, the boundary layer, and the distance from the body to the rear face of the shock (Δ). When the boundary and shock layers merge, these three divisions no longer have any significance as separate entities. For this reason, the shock detachment distance, Δ, is taken to be the distance from the face of the body to the shock leading edge.

4.1.3 Flat-Faced Body Results

Some limited tests were made with two water-cooled, flat-faced probes at the same flow conditions as for the water-cooled spheres. The results of the tests are shown in Fig. 3. No attempt has been made to draw a single curve through these results since the sphere data imply that there will be a variation with Mach number, which the limited nature of these tests of flat-faced bodies cannot fully specify.

The results of this test are interesting when they are considered in conjunction with the sphere data. First of all, the shock detachment distance is more than twice the value obtained for a sphere at the same Mach number and Reynolds number. This implies that, provided the boundary layer increases in the same manner as for a sphere, the boundary and shock layers will not merge until a lower Reynolds number than that at which merging occurs for a sphere is reached. Thus, incipient and merged-layer phenomena would not be expected to occur with flat-face bodies until a lower Reynolds number than that at which they occur for

spheres is reached. In connection with this, Sherman's (Ref. 16) work on impact-pressure probes shows that the rapid increase in impact pressure of Reynolds number occurs at higher Reynolds number for source-shaped probes than for flat-faced probes. This is consistent with the idea that merged-layer characteristics occur at higher Reynolds number for source-shaped than for flat-faced probes.

It has been shown that shock detachment distance is a function of wall temperature, among other things. In Ref. 17, a study was made of flat-faced, impact-pressure probes where the wall to stagnation temperature ratio was approximately 0.3. It was found that these results did not compare very well with some data obtained for a wall to stagnation temperature ratio of unity. The present investigation would seem to indicate that this difference could be at least partly accounted for by the difference in shock detachment distance for the two cases. Van Dyke (Ref. 1) has shown that shock detachment distance is primarily a function of the density ratio across a normal shock wave. For a sphere, the effect of different specific heat ratios is small. For the density ratios of the present tests, the error involved in the shock detachment distance by taking $\gamma = 1.4$ instead of 1.667 is on the order of 3 percent. Assuming that the same is true for flat-faced bodies, then a good approximation to the inviscid value of Δ/R_b for the flat-faced bodies can be obtained from experimental data for flat-faced bodies, and this is shown in Fig. 8. The inviscid values of Δ/R_b for the density ratios of the present tests are shown in Fig. 3. As for the spheres, there is an indication that for the Reynolds numbers of the present tests the measured value of Δ/R_b is less than the inviscid value through an intermediate range of Reynolds numbers.

4.2 SHOCK SHAPE

4.2.1 Sphere Results

The results of the analysis to determine the shock shape are shown in Figs. 9 and 10. For the range of Mach number and Reynolds number of these tests, the nondimensionalized shock shape is a function of Mach number only, after the effect of Reynolds number on Δ is accounted for. In order to account for the Reynolds number effect on the shock detachment distance, Δ, the origin of the ordinates is taken to be at the apex of the shock-wave profile.

In Ref. 18, an analysis of experimentally determined shock shapes has shown that these shapes could be represented by an equation of hyperbolic form:

$$y/D = A\left[\left(\frac{x}{D}\right)^{\frac{i}{n}} + a\left(\frac{x}{d}\right)\right]^{n} \qquad (6)$$

with the apex at the origin and with A being the slope of the asymptotic shock angle far from the body. When n = 1/2, this equation is exactly hyperbolic. From the above-mentioned shock-shape analysis, values were assigned to A, n, and a and were shown to be functions of free-stream Mach number and the nose wave drag coefficient, calculated by using the modified Newtonian approximation and the specific heat ratio of the gas. On comparing the shock shapes predicted by this method with those calculated by an empirical relationship by Love (Ref. 19), it was found that Love's method gave a better prediction for Mach numbers less than four. The empirical relationships derived in Refs. 18 and 19 are for air only, and neither of them can be simply modified to account for a gas with a specific heat ratio other than 1.4. It has been shown in Ref. 6 that the blast analogy is a useful means for predicting some of the features of hypersonic flow over blunt bodies. In fact, it is possible with this method to predict the relative effects of, say, a change in specific heat ratio very well, while being unable to predict a precise value of the quantity under investigation. In terms of the blast analogy, the shock shape in front of a body can be written as:

$$(y/D)_{M_\infty >> 1} \simeq \left(\frac{\gamma_\infty C_D}{4 j_o}\right)^{1/4} \left(\frac{x_b}{D}\right)^{1/2} \tag{7}$$

This is a useful form when a comparison of the effects of different specific heat ratios on shock shape is to be made. When the relevant values of the specific heat ratio for air and argon are substituted in this equation at constant value of x_b/D, the ratio $(y/D)_{argon}/(y/D)_{air} = 1.16$. Some experimental results for helium (Refs. 20 and 21), which has the same specific heat ratio as argon over a Mach number range from 15 to 40, show that this ratio is 1.17.

For the present Mach number range of 4.22 to 9.21, the method given in Ref. 19 has been used to determine the shock shape for spherical bodies in air. The data for Mach numbers of 8.61 and 9.21 were obtained by extrapolating the results contained in Ref. 19. It was considered that this was preferable to using another method, say Ref. 18, to calculate the shock shape at these high Mach numbers. The resulting shock shapes are shown plotted in Figs. 9 and 10. The ratio $(y/D)_{argon}/(y/D)_{air}$ derived from the experimental argon data and the calculated air data is shown plotted against Mach number in Fig. 11. At the high Mach number end of this curve, this ratio agrees very well with the blast analogy. Intuitively, it would seem that the ratio must decrease with decreasing Mach number. No reason can be found for the abrupt change in slope of the curve at a Mach number of approximately six.

4.2.2 Flat-Faced Results

The measured shock shapes for the flat-faced bodies are shown in Fig. 12. The shock shapes shown for air were derived from some experimental data for flat-faced bodies contained in Refs. 19 and 22. Equation (7) indicates that the ratio $(y/D)_{argon}/(y/D)_{air}$ should be the same for spheres and for flat-faced bodies. The dashed lines in Fig. 12 were obtained by using the experimentally determined curves for air and multiplying them by the experimentally determined ratio in Fig. 11. It will be seen that the dashed curves fit the experimentally measured shock shapes for flat-faced bodies, which provides additional confirmation of the form of the curve shown in Fig. 11.

4.2.3 Correlation of Shock Shapes

In terms of the blast analogy the parameter governing the form of the shock-wave shape at high Mach numbers is given by Eq. (7) as $(x_b/D)C_D^{1/2}$ for a constant value of γ. For Mach numbers greater than 4.0 the inviscid drag coefficient of both flat-faced bodies and spheres is approximately constant. Therefore, to correlate the experimental shock shape data for spheres and flat-faced bodies, it should be sufficient to plot x/D versus y/D on log-log paper. Figure 13 shows the result of plotting data obtained from the faired curves of Figs. 9, 10, and 12, for both argon and air. The fact that a series of parallel straight lines can be drawn through the sphere data indicates that a constant value can be given to the exponent of (x_b/D) in Eq. (7). However, $(\gamma_\infty C_D/4J_o)$ will be a function of Mach number for $M_\infty < 6$, a fact which is not predicted by the blast analogy which applies to hypersonic flows. A straight line cannot be drawn through the flat-faced body data for values of $x/D < 1.0$, which means that a constant value cannot be assigned to the exponent in Eq. (7). There are insufficient data to say definitely whether there is a linear relationship between x/D and y/D for values of $y/D > 1.0$, though there are indications to suggest that this is so.

4.3 SHOCK-WAVE THICKNESS

In Section 4.1.2, a theory derived by Ziering, et al. (Ref. 11), for monatomic gases was used to estimate the thickness of the shock wave for the present tests. This estimate was chosen because it appeared to be in reasonable agreement with the experimental data for Mach numbers up to 5. A comparison of some of the theoretical estimates of shock-wave thickness for monatomic gases is shown in Fig. 14 together with the experimental data published by other investigators.

In the calculation of the shock-wave thickness, two approaches have been used. In one, the Navier-Stokes equations have been used to calculate

shock-wave profiles, and curve 6 in Fig. 14 shows a solution by Schwartz, as reported by Hornig in Ref. 23. The other solutions are developments of a method suggested by Mott-Smith (Ref. 24) for the solution of the Boltzmann equation. Curves 1-5 in Fig. 14 (Refs. 11, 23, 25-27) give the results of calculations of this form. For Mach numbers less than approximately two, all of the calculations are in reasonable agreement with the available experimental data. However, for higher Mach numbers, the degree of agreement is poor. At a Mach number of six, the solution proposed by Koga gives a value of the shock thickness five times larger than that predicted by the Navier-Stokes equations, with the other solutions lying within this range.

By far the most consistent and extensive set of experimental data to date is that by Linzer, reported by Hornig in Ref. 23. These values of shock-wave thickness have been derived from measurements of the optical reflectivity of the shock wave. Although most of the other test data reported in Ref. 28 are in good agreement with the above data at low Mach numbers, there is some scatter in the data at the higher Mach numbers. In spite of this scatter, it seems fair to conclude from the experimental data that the shock-wave thickness has a minimum value at $M \approx 3.5$ and thereafter increases with increase in Mach number. This form of variation is the same as that predicted by Ziering, et al. (Ref. 11), although the actual values of the shock thickness are not the same.

It is important to remember that the shock-wave thickness considered here is the thickness of the density profile. Furthermore, the thicknesses quoted are the maximum slope thicknesses of this profile, as illustrated in Fig. 15. Sherman (Ref. 29) has shown that there is considerable difference between the total shock-wave thickness and the maximum slope thickness in the low-density flow regime. In fact, when consideration is being given to the merging of shock and boundary layers in front of a blunt body, it would seem that the total thickness is more significant than the maximum slope thickness.

Consider the structure of the shock wave at locations removed from the spheres and flat-faced bodies of the present tests. If it is assumed that the film density of the photographic negatives is proportional to the density in the gas flow, then the measurement of the film density with the photo-densitometer should give the form of the density variation throughout the flow regime under investigation. As stated earlier for all the flow conditions investigated herein, there is an axial Mach number gradient, which in turn implies a density gradient. Measurement of the film density upstream of the body shock indicates that the film density decreases as the shock is approached, i.e., in passing downstream. Furthermore,

the rate of decrease of film density decreases as the region of flow under investigation moves farther and farther downstream from the nozzle exit. This implies a decrease of axial Mach number gradient as the distance from the nozzle exit plane increases. This is consistent with the results of the nozzle calibration studies which show just such a decreasing gradient.

The film density of a large number of the negatives was recorded on the strip chart recorder attached to the photo-densitometer for a series of stations along the bow shock, but sufficiently far from the bodies to avoid boundary-layer influences. As the shock was approached from upstream, the density decreased, then underwent a gradual increase at the front of the shock, then a rapid rise, then a more gradual rise, then became almost constant, and finally the density started to decrease. An example is shown in Fig. 16. Consider the density variation along section AA through the three-dimensional shock shown in Fig. 17. From a-b, the density decreases because of the axial Mach number gradient; from b-c-d, an increase occurs in density through the shock to a maximum value at d at the rear face of the shock; and from d-e, a decrease in density occurs because of the flow expansion behind the shock. The form of this density variation is the same as that recorded by the photo-densitometer in Fig. 16. Now, if the radiation of light from the shock wave is considered, it will be seen that the maximum section length through the shock wave occurs at section d. This indicates that the points of maximum film density and flow density can occur at the same points. By adjusting the rate at which the carriage carrying the negative is passed by the viewing slit of the densitometer, the shock thickness recorded on the strip chart recorder can extend over several inches. Both the maximum slope and total thickness of the shock waves were measured from this recorded data. These thicknesses were measured normal to the tangent to the shock wave. Then, taking the free-stream mean free path and Mach number resolved in a direction normal to the shock wave, the ratio of the maximum slope shock-wave thickness to the free-stream mean free path was calculated and is shown plotted in Fig. 18. The scatter in the data is on the order of ±10 percent. This shows that as the Mach number increases above roughly three, the shock-wave thickness increases, which is in agreement with the form predicted in Ref. 11. An attempt has been made to estimate the total thickness even though it was difficult to define exactly where the edges of the shock wave were. Figure 18 shows that the total thickness is approximately 50 percent greater than the maximum slope thickness. Sherman (Ref. 29) has made a study of the shock-wave thickness using a fine wire probe (which was essentially a free-molecule flow probe) in helium and air. The results of this study in the Mach number range from 1.72 to 3.91 show that the total thickness is always approximately double the maximum slope thickness. Also of interest

is the fact that in this study the wire temperature profile is not symmetrical about the mean temperature value. Some of the film density profiles obtained in the present tests were also of this form. Hornig (Ref. 23) indicates that theory predicts that this asymmetry is a property of strong shocks. It would seem from the present results and those of Sherman that this property of strong shock waves is confirmed. As mentioned by Hornig, such a property of shock waves poses a problem in the optical reflectivity method of shock-wave thickness measurements, since the basis for the method is the assumption that the density profile through the shock is symmetrical.

4.4 SPHERE PRESSURE DISTRIBUTIONS

Surface pressure distributions in the Mach number range from 4.4 to 13.5 are shown in Fig. 19 and Table 1. A comparison is made with the modified Newtonian approximation:

$$C_p = C_{p_{max}} \cos^2 \theta \tag{8}$$

This equation can be rewritten in terms of surface pressure and the pressure at the stagnation point:

$$\frac{p}{p_o'} = \cos^2 \theta + \frac{p_\infty}{p_o'} \sin^2 \theta \tag{9}$$

For the complete Mach and Reynolds number range of these tests, the modified Newtonian approximation gives a good prediction of the surface pressure distribution up to an angle of 60 deg. Above 60 deg, there is a tendency for the modified Newtonian approximation to underestimate the surface pressure distribution. However, it must be emphasized that the degree of disagreement between theory and experiment is small even at surface angles greater than 60 deg.

Talbot, et al. (Ref. 30), have shown for hemispherically blunted cones in an unheated, low-density flow that the modified Newtonian approximation gives good results over the hemispherical part of the body. Hayes and Probstein (Ref. 31), in a comparison of the merits of the various methods of predicting the surface pressure distribution over spheres, emphasize that the modified Newtonian approximation is strictly an empirical formula. A more rational estimate is the Newton-Busemann law which takes into account centrifugal effects:

$$\frac{p}{p_o'} = 1 - \frac{4}{3} \sin^2 \theta \tag{10}$$

This law, though more rational in nature than the modified Newtonian approximation, gives poor agreement with experiment. Hayes and

Probstein (Ref. 31) consider that the good results obtained with the modified Newtonian approximation are fortuitous and that the centrifugal pressure difference across the shock layer is in many instances offset by the effect of the difference in the shock and body angles.

Perhaps one of the more interesting results from this experiment is that the modified Newtonian theory is valid in a region where the shock and boundary layers merge. The only other known data in the low-density regime where the shock and boundary layers had not merged are contained in Ref. 30.

It is of interest to consider the form of the surface pressure distribution in the free-molecule flow regime in order to determine how the form of the distribution changes in going from the continuum to free-molecule regimes. The surface pressure distribution of a sphere in the free-molecule flow regime, given in Ref. 32, is

$$\frac{p}{p_\infty}\sqrt{\frac{T_\infty}{T}} = \left[e^{-S^2\cos^2\theta} + \sqrt{\pi}\, S\cos\theta\,(1 + \operatorname{erf} S\cos\theta)\right] \tag{11}$$

If the pressure at the stagnation point is written as p_o', then the pressure at any point on the sphere can be written as

$$\frac{p}{p_o'} = \frac{\left[e^{-S^2\cos^2\theta} + \sqrt{\pi}\, S\cos\theta\,(1 + \operatorname{erf} S\cos\theta)\right]}{\left[e^{-S^2} + \sqrt{\pi}\, S\,(1 + \operatorname{erf} S)\right]} \tag{12}$$

for $S\cos\theta \geq 2.0$

then $\operatorname{erf} S\cos\theta \to 1.0$

then Eq. (16) becomes

$$\left(\frac{p}{p_o'}\right) \approx \cos\theta \quad \text{when} \quad S\cos\theta \geq 2 \tag{13}$$

For the present series of tests, this would imply that if any free-molecule flow effects were present, the measured pressures would be larger than those predicted by the modified Newtonian approximation. Since the measured pressures are not larger than those predicted by the modified Newtonian approximation, then the spheres are not being affected by any free-molecule flow effects. This is not a surprising result when it is considered that the largest Knudsen number, based on sphere radius, of the present tests is approximately 0.07 for a billiard-ball molecular model.

5.0 CONCLUSIONS

Based on an experimental investigation to determine the pressure distribution, shock shape, and shock detachment distance for spheres and the latter two characteristics for flat-faced bodies in heated argon flow, the following conclusions are made:

The shock detachment distance in front of a body in low-density, hypervelocity flow is a function of Mach number, wall-to-stagnation temperature ratio, and Reynolds number and body shape. Evidence from the results of the present series of experiments suggests that the shock wave and boundary layers in front of the bodies were merged.

For complete range of Mach and Reynolds numbers encountered in this experiment, the nondimensionalized shock shape was a function of Mach number and body shape only. Furthermore, the difference between the shock shapes in air and argon at high Mach numbers was in very good agreement with that predicted by the blast analogy.

Even in the flow regime where the shock and boundary layers were merged, the modified Newtonian approximation gave good results for the surface pressure distribution over spheres for $\theta \leq 60$ deg.

Measurements of shock-wave thickness in the low-density regime were in reasonable agreement with results at higher densities when ratioed to mean free path. Also, the form of the variation of shock-wave thickness with Mach number agreed with that predicted by Ziering, et al. (Ref. 11).

REFERENCES

1. Van Dyke, Milton D. and Gordon, Helen D. "Supersonic Flow Past a Family of Blunt Axisymmetric Bodies." NASA Technical Report R-1, 1959.

2. Probstein, Ronald F. and Kemp, Nelson H. "Viscous Aerodynamic Characteristics in Hypersonic Rarefied Gas Flow." Journal of the Aero/Space Sciences, Vol. 27, No. 3, March 1960, pp. 174-192, 218.

3. Ho, Hung-Ta and Probstein, Ronald F. "The Compressible Viscous Layer in Rarefied Hypersonic Flow." Brown University, ARL-TN-60-132.

4. Levinsky, E. S. and Yoshihara, H. "Rarefied Hypersonic Flow Over a Sphere." Hypersonic Flow Research, Progress in Astronautics and Rocketry, Vol. 7, August 16-18, 1961, Academic Press, New York, 1962, pp. 81-106.

5. Moulic, E. S. "Afterflow Investigations of Shock Detachment Distances at Low Reynolds Numbers." WADC Technical Report 57-643, July 15, 1958.

6. Lukasiewicz, J. "Hypersonic Flow-Blast Analogy." AEDC-TR-61-4, June 1961.

7. Boison, J. Christopher and Curtiss, Howard A. "An Experimental Investigation of Blunt Body Stagnation Point Velocity Gradient." ARS Journal, Vol. 29, No. 2, February 1959, pp. 130-135.

8. Potter, J. L., Kinslow, M., Arney, G. D. Jr., and Bailey, A. B. "Description and Preliminary Calibration of a Low-Density Hypervelocity Wind Tunnel." AEDC-TN-61-83, August 1961.

9. Bailey, A. B. and Boylan, D. E. "Some Experiments on Impact-Pressure Probes in a Low-Density, Hypervelocity Flow." AEDC-TN-61-161, December 1961.

10. Berndt, S. B. "On the Influence of the Non-Uniform Free-Stream of a Conical Wind Tunnel Nozzle on the Axisymmetric Hypersonic Flow Around Blunt Bodies." National Research Council of Canada, NRC-LR-338, February 1962.

11. Ziering, S., Ek, F., and Koch, P. "Two-Fluid Model for the Structure of Neutral Shock Waves." The Physics of Fluids, Vol. 4, No. 8, August 1961, pp. 975-987.

12. Cohen, C. B. and Reshotko, E. "The Compressible Laminar Boundary Layer with Heat Transfer and Arbitrary Pressure Gradient." NACA Report 1294, 1956.

13. Stoddard, F. J. "Stagnation Point Viscous Hypersonic Flow." Journal of the Aero/Space Sciences, Vol. 29, No. 9, September 1962, Readers Forum, pp. 1138-1139.

14. Schwartz, R. N. and Eckerman, J. "Shock Location in Front of a Sphere as a Measure of Real Gas Effects." Journal of Applied Physics, Vol. 27, No. 2, February 1956, pp. 169-174.

15. Vas, I. E., Bogdonoff, S. M., and Hammitt, A. G. "An Experimental Investigation of the Flow Over Simple Two-dimensional and Axial Symmetric Bodies at Hypersonic Speeds." Jet Propulsion, Vol. 28, No. 2, February 1958, pp. 97-104.

16. Sherman, F. S. "New Experiments on Impact-Pressure Interpretation in Supersonic and Subsonic Rarefied Air Streams." NACA-TN-2995, September 1953.

17. Bailey, A. B. "Further Experiments on Impact-Pressure Probes in a Low-Density, Hypervelocity Flow." AEDC-TDR-62-208, November 1962.

18. James, Carlton S. and Terry, James E. "Shock-Wave Profiles Over Ellipsoidal-Nosed Bodies in Hypersonic Flow." Journal of the Aero/Space Sciences, Vol. 29, No. 9, September 1962, Readers' Forum, pp. 1128-1129.

19. Love, Eugene S. "A Re-examination of the Use of Simple Concepts for Predicting the Shape and Location of Detached Shock Waves." NACA-TN-4170, December 1957.

20. Van Hise, Vernon. "Analytic Study of Induced Pressure on Long Bodies of Revolution with Varying Nose Bluntness at Hypersonic Speeds." NASA-TR-R-78, May 1961.

21. Inouye, Mamoru and Lomax, Harvard. "Comparison of Experimental and Numerical Results for the Flow of a Perfect Gas about Blunt-Nosed Bodies." NASA-TN-D-1426, September 1962.

22. Chones, A. J. "Heat Transfer and Pressure Measurements on Flat-Faced Flared-Tail Circular Cylinders and Normal Disks." U. S. Naval Ordnance Laboratory, NAVORD Report 6669, June 15, 1959.

23. Hornig, D. F. "Energy Exchange in Shock and Detonation Waves." Frick Chemical Laboratory, Princeton University, Tech. Rept. No. 4, October 1962.

24. Mott-Smith, H. M. "The Solution of the Boltzmann Equation for a Shock Wave." Phys. Review, Ser. 2, Vol. 82, No. 6, June 15, 1951, pp. 885-892.

25. Koga, T. "The Structure of Strong Shock Waves of Stable Monatomic Molecules." Rarefied Gas Dynamics (L. Talbot, ed.), Academic Press, New York, pp. 481-499.

26. Muckenfuss, C. "Bimodal Model for Shock Wave Structure." The Physics of Fluids, Vol. 3, No. 3, March 1960.

27. Glandsdorff, P. "Solution of the Boltzmann Equations for Strong Shock Waves by the Two-Fluid Model." The Physics of Fluids, Vol. 5, No. 4, April 1962.

28. Losev, S. A. and Osipov, A. I. "The Study of Non-Equilibrium Phenomena in Shock Waves." A translation of "Advances in the Physical Sciences" of the Academy of Sciences of the USSR, Published by the American Institute of Physics Incorporated, Vol. 4, No. 4, January-February 1962.

29. Sherman, F. S. "A Low-Density Wind-Tunnel Study of Shock-Wave Structure and Relaxation Phenomena in Gases." NACA-TN-3298, July 1955.

30. Talbot, L., Schaaf, S. A., and Hurlbut, F. C. "Pressure Distributions on Blunt-Nosed Cones in Low Density Hypersonic Flow." Jet Propulsion, Vol. 28, No. 12, December 1958, pp. 832-834.

31. Hayes, Wallace D. and Probstein, Ronald F. Hypersonic Flow Theory. Academic Press, New York and London, 1959, p. 243.

32. Patterson, G. N. "Mechanics of Rarefied Gases and Plasmas." UTIA Review No. 18, March 1962.

TABLE 1

FLOW CONDITIONS FOR PRESSURE DISTRIBUTION TESTS ON A 0.50-IN.-DIAM., WATER-COOLED SPHERE

Tabulated Values of p/p_o' for Various Angles

M	T_o, °K	p_o Abs., lb/in.^{2}	Re_∞/in., in.$^{-1}$	Re_2/in., in.$^{-1}$	λ_∞, in.	15°	30°	45°	60°	75°	90°	100°
5.95	1938	2.025	2115	344	0.00482	0.926	0.766	0.527	0.232	0.122	0.0330	------
4.38	2780	1.015	895	249	0.00800	0.936	0.723	0.509	0.271	0.143	0.0477	0.0247
4.95	2780	1.015	790	187	0.01077	0.931	0.705	0.505	0.270	0.138	0.0459	0.0236
5.55	2780	1.015	675	136	0.01363	0.918	0.706	0.500	0.267	0.135	0.0442	0.0211
6.15	2780	1.015	625	108	0.01653	0.937	0.711	0.496	0.258	0.123	0.0409	0.0195
12.2	2853	6.0	1765	86.6	0.00982	0.952	0.741	0.513	-----	-----	------	------
4.4	2918	2.05	1600	445	0.00421	0.934	0.730	0.524	0.264	0.143	0.0474	0.0266
5.18	2918	2.05	1400	313	0.00628	0.919	0.711	0.516	0.266	0.143	0.0464	0.0256
5.83	2918	2.05	1205	228	0.00814	0.927	0.706	0.509	0.266	0.143	0.0452	0.0249
6.45	2918	2.05	980	158	0.01004	0.928	0.710	0.518	0.272	0.143	0.0423	0.0281
8.65	3020	3.33	1220	120	0.01176	0.912	0.737	0.489	-----	-----	0.0397	0.0190
9.25	3059	5.55	1890	164	0.00813	0.933	0.741	0.493	-----	-----	0.0418	0.0189
11.5	3070	4.31	1200	68.5	0.01506	0.919	0.736	0.493	0.251	0.141	0.0320	------
13.5	3075	5.55	1320	54.8	0.01281	0.890	0.721	0.507	-----	-----	0.0512	0.0282
6.29	3088	4.31	2175	370	0.00479	0.934	0.790	0.530	0.235	0.122	0.0310	------
5.95	3150	2.575	1355	252	0.00728	0.924	0.770	0.497	0.229	0.121	0.0300	------
6.06	3180	1.94	985	178	0.01151	0.939	0.737	0.486	-----	-----	0.0393	0.0181
5.98	3642	2.775	1195	225	0.00823	0.928	0.777	0.507	0.230	0.122	0.0300	------
5.36	4020	1.165	515	113	0.01740	0.931	0.729	0.489	-----	-----	0.0324	0.0120

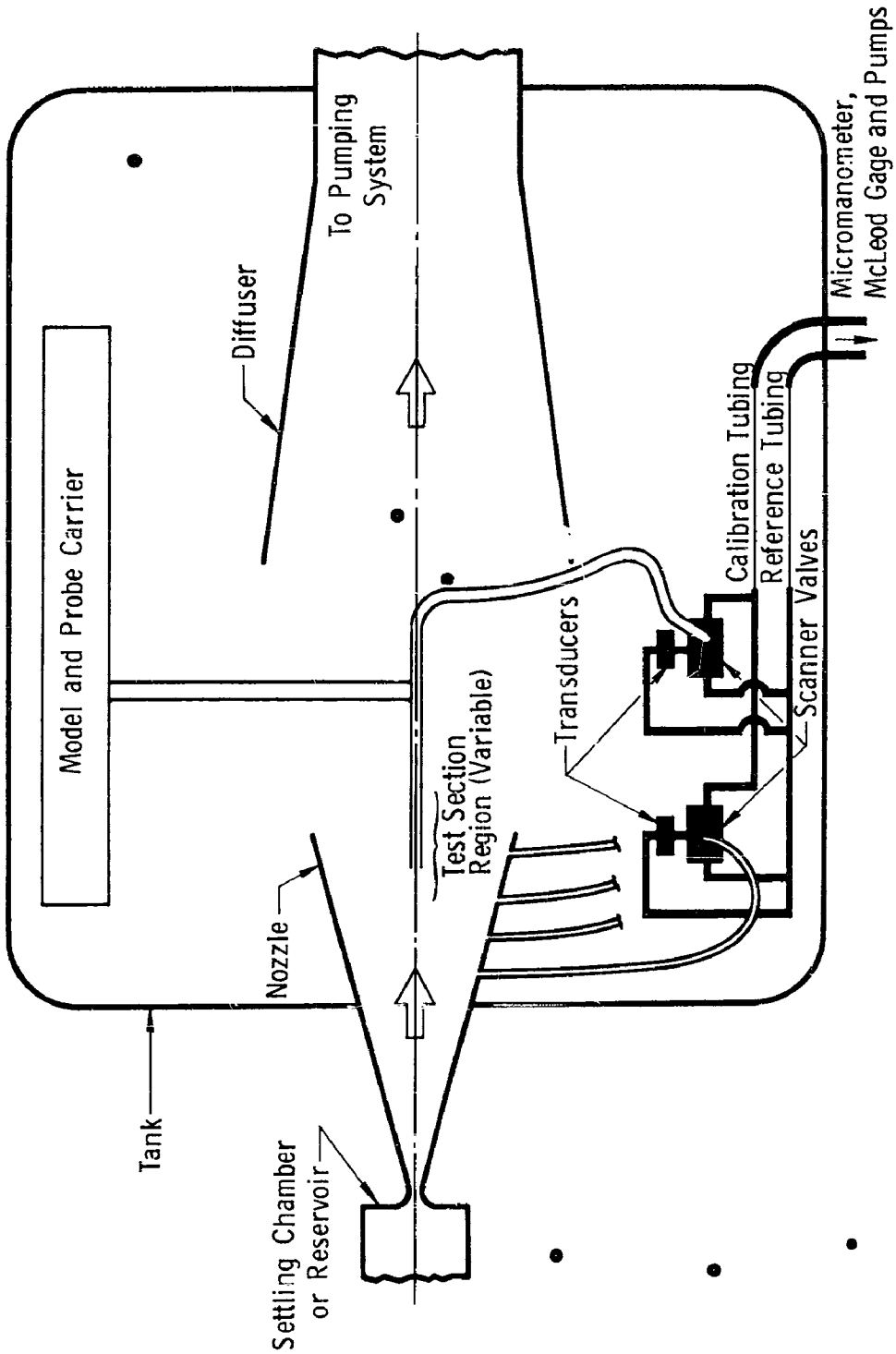

Fig. 1 Schematic Drawing of LDH Tunnel Nozzle, Tank, and Diffuser Area (Not to Scale)

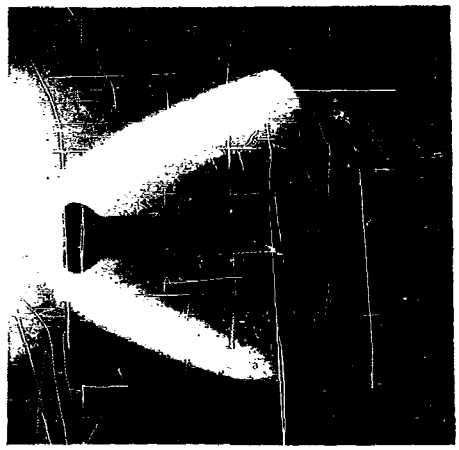

M_∞ 4.73
T_o 2780°K
Re_2/in. 212
D 0.249 in.

M_∞ 6.23
T_o 2990°K
Re_2/in. 334
D 0.688 in.

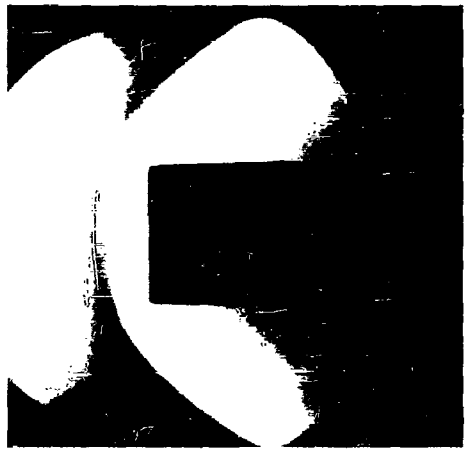

M_∞ 4.73
T_o 2780°K
Re_2/in. 212
D 0.497 in.

Fig. 2 Flow over Spheres and Flat-Faced Bodies

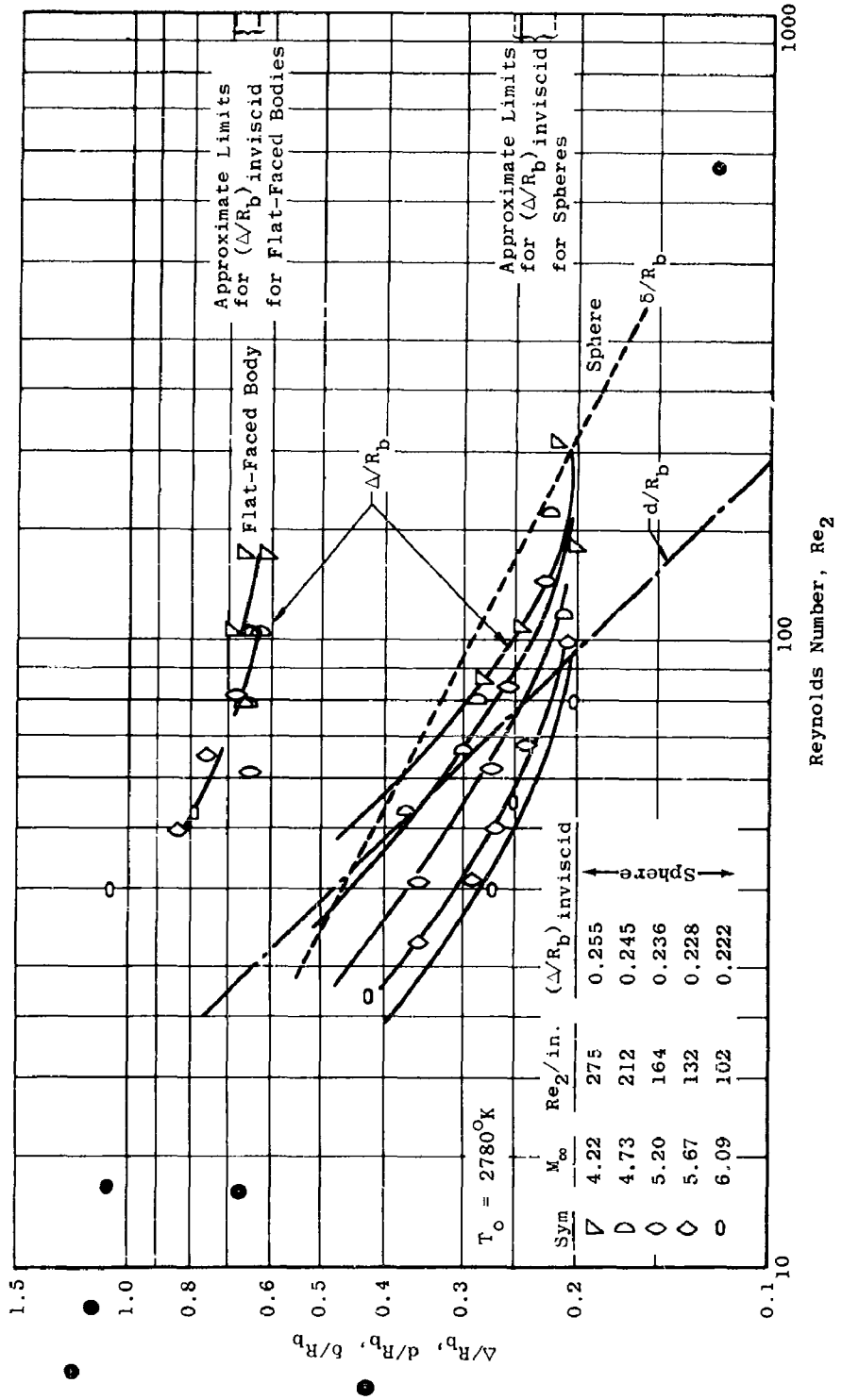

Fig. 3 Stagnation Region Shock Detachment Distance for a Water-Cooled Sphere and Flat-Faced Body in Argon ($T_w/T_o \simeq 0.11$)

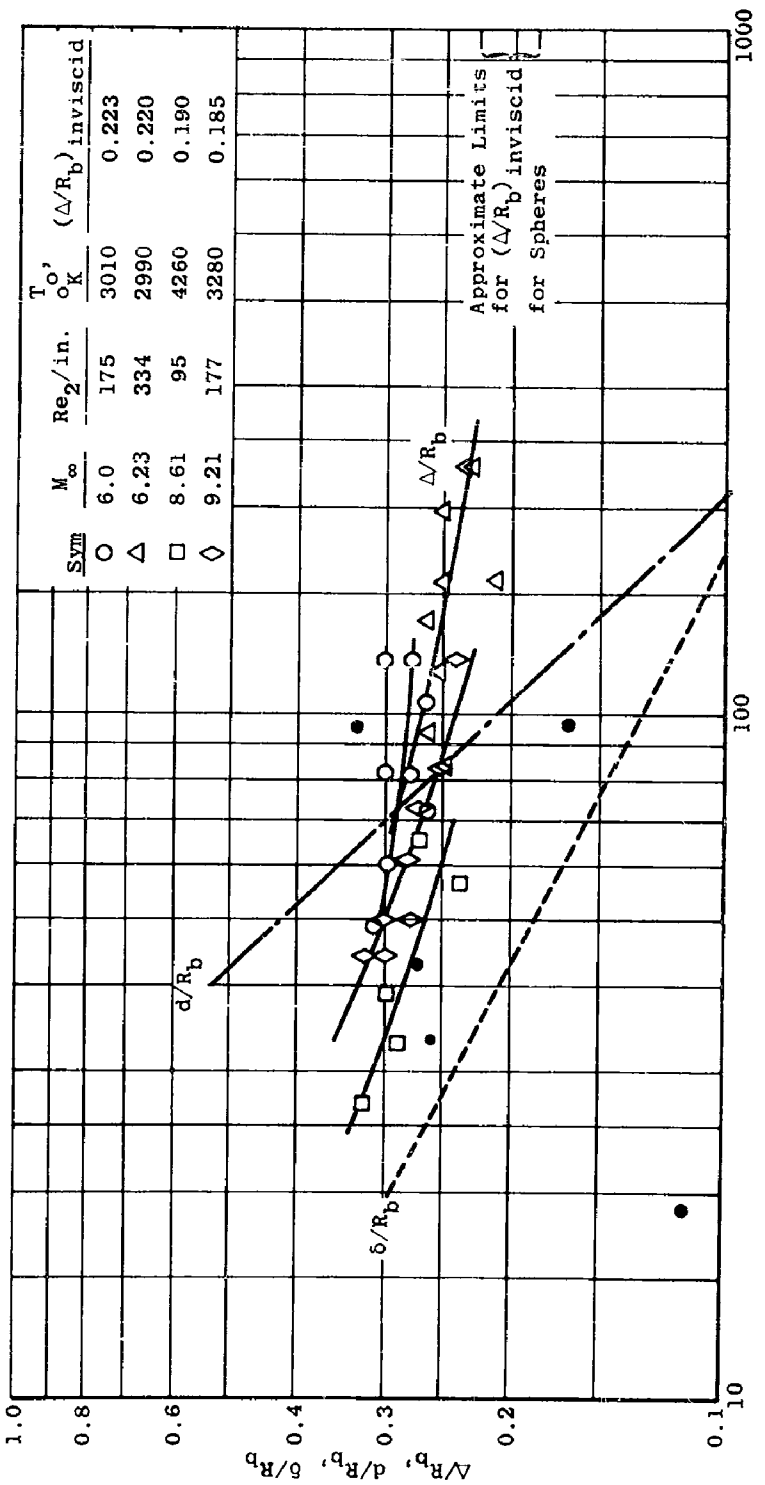

Fig. 4 Stagnation Region Shock Detachment Distance for a Sphere in Argon ($0.24 \leq T_w/T_o \leq 0.33$)

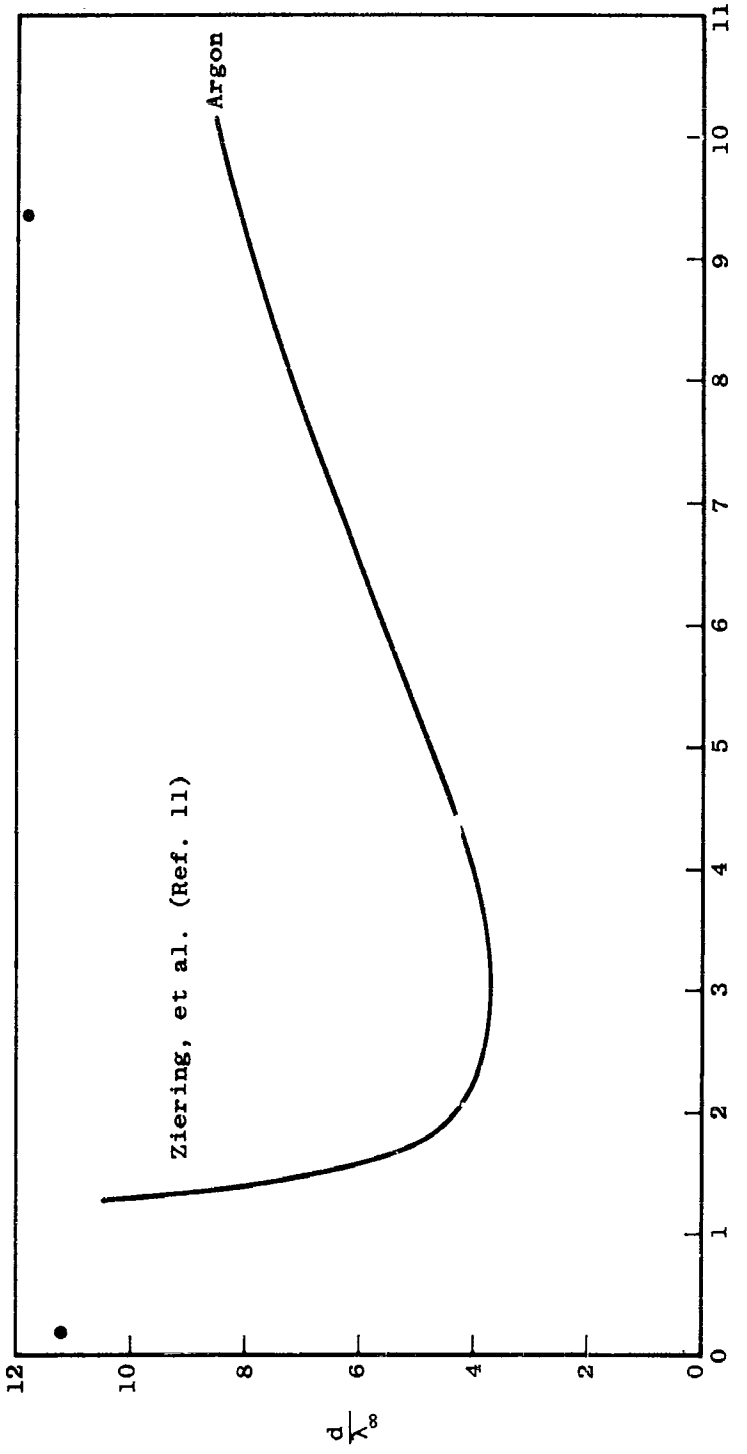

Fig. 5 Variation of Shock-Wave Thickness with Mach Number

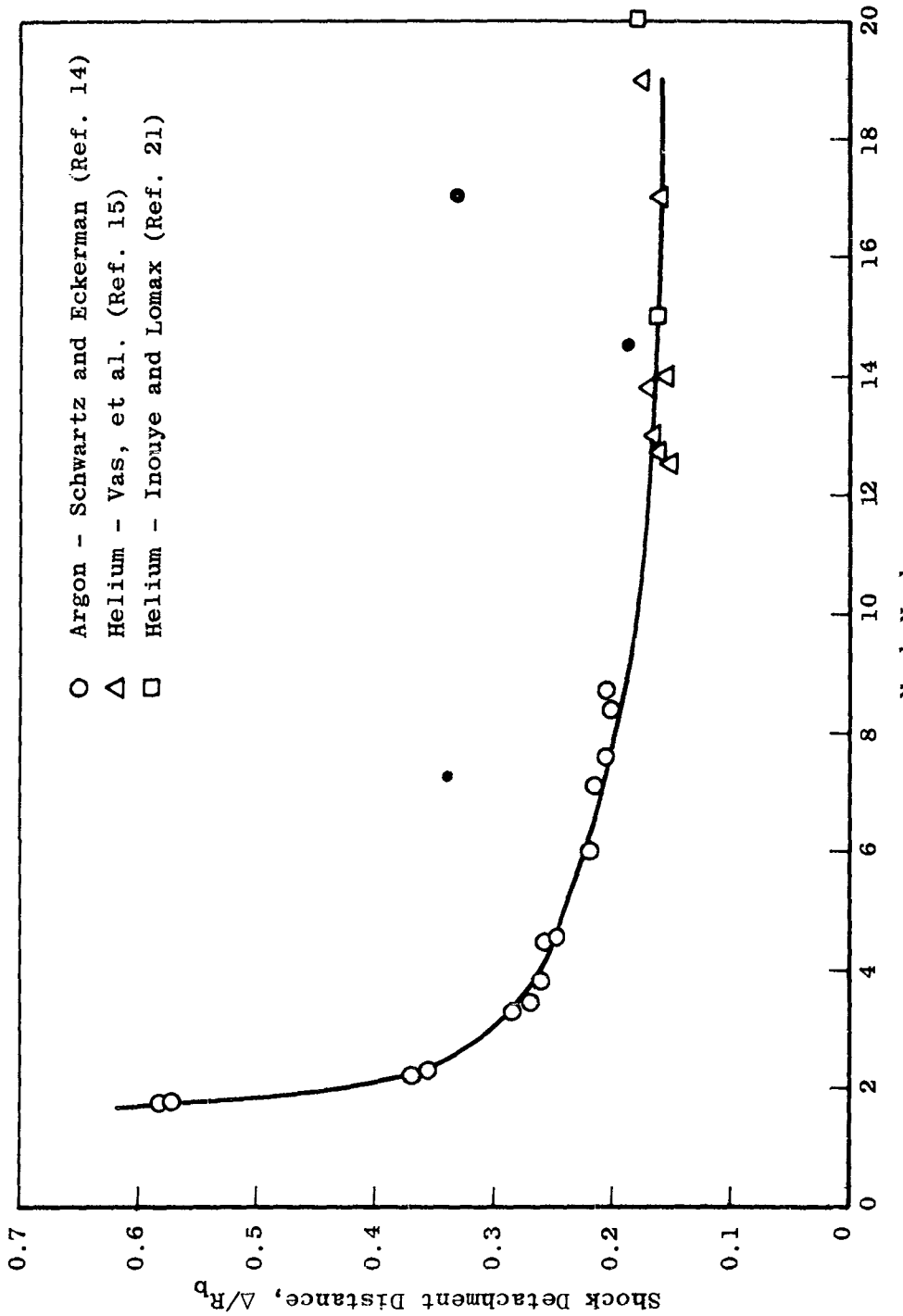

Fig. 6 Shock Detachment Distance for a Sphere in a Monatomic Gas at High Reynolds Number

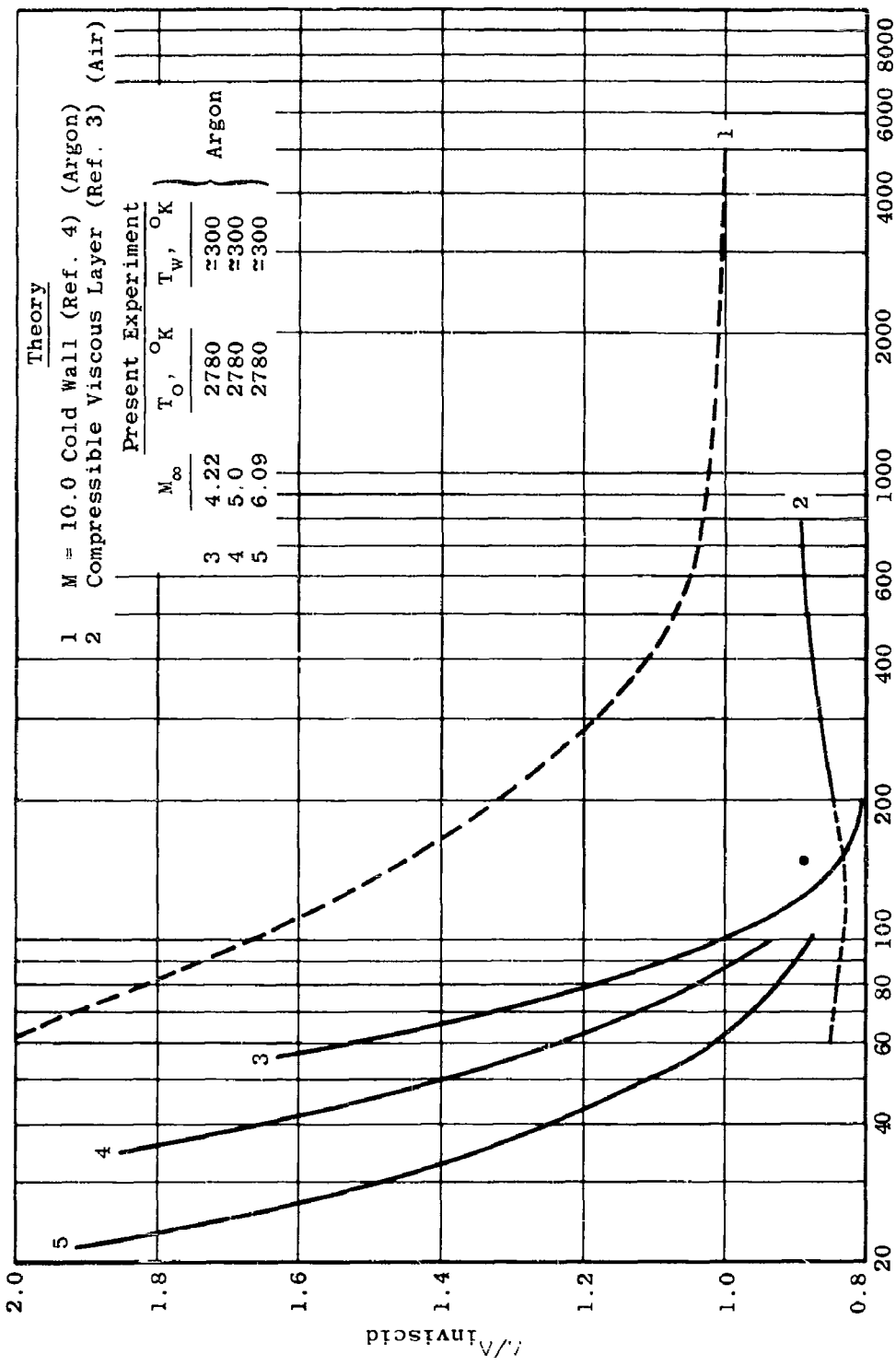

Fig. 7 Comparison of Theoretical and Experimental Shock Detachment Distances

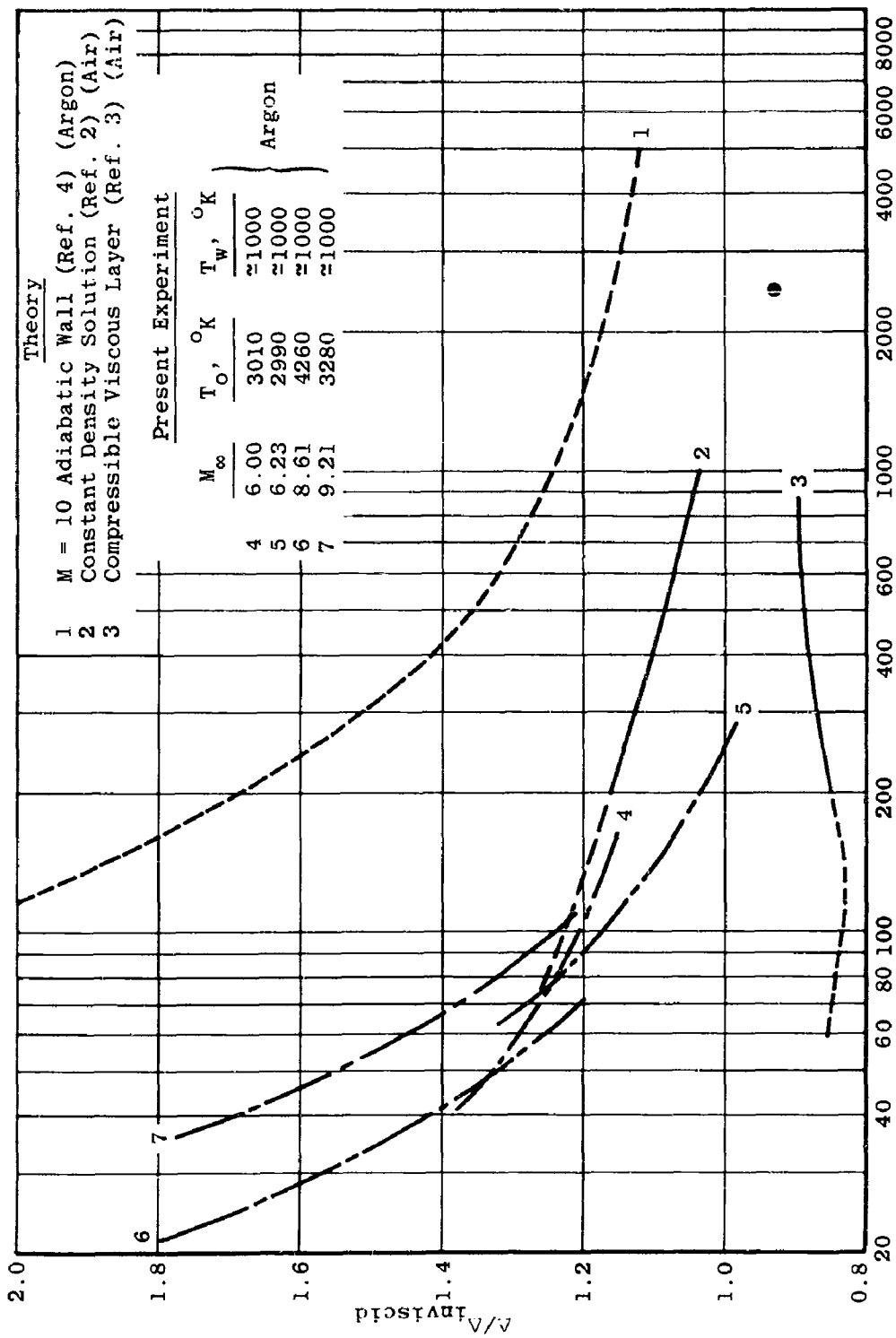

Fig. 7 Concluded

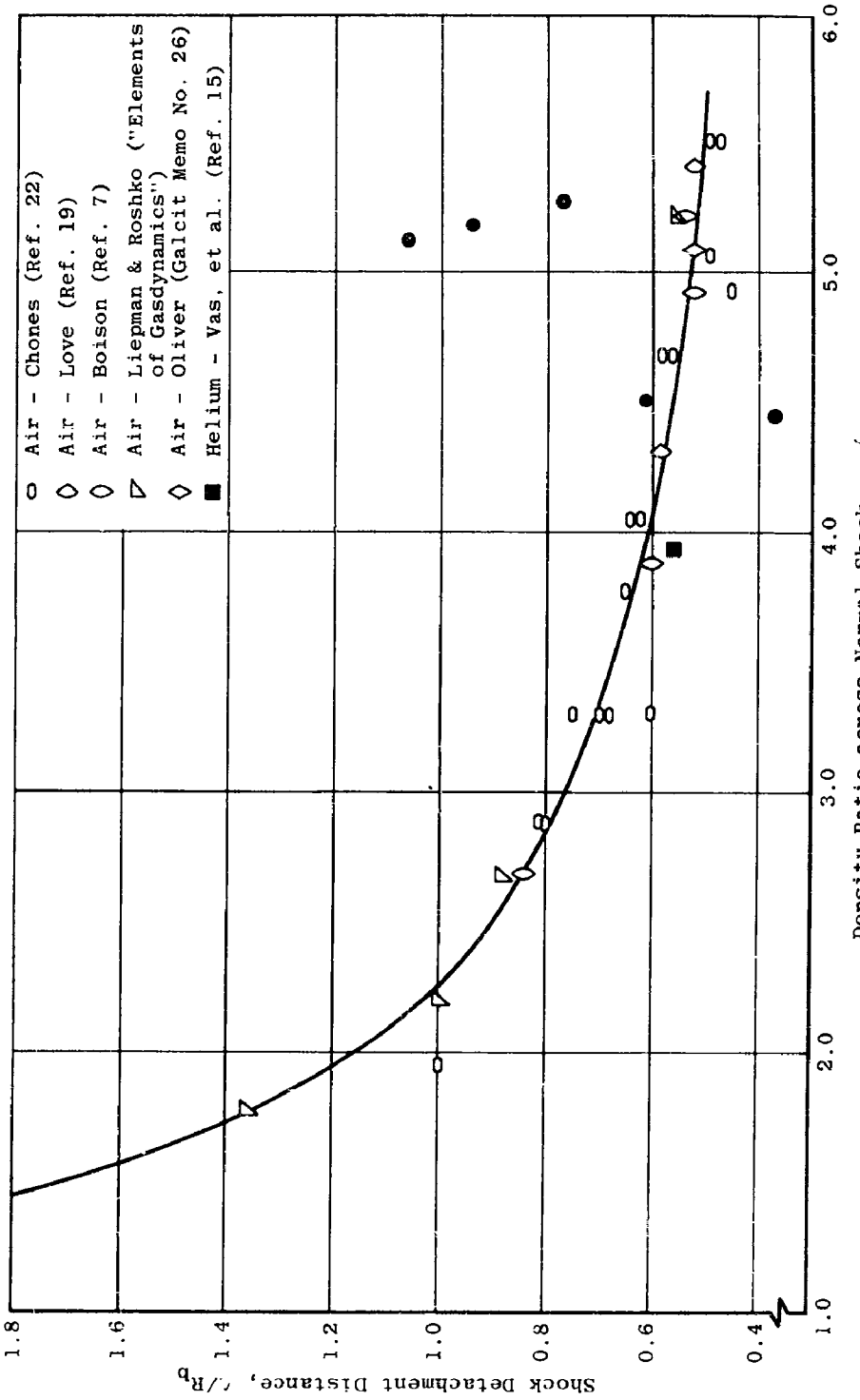

Fig. 8 The Shock Detachment Distance as a Function of Density Ratio across a Normal Shock for a Flat-Faced Body at High Reynolds Number

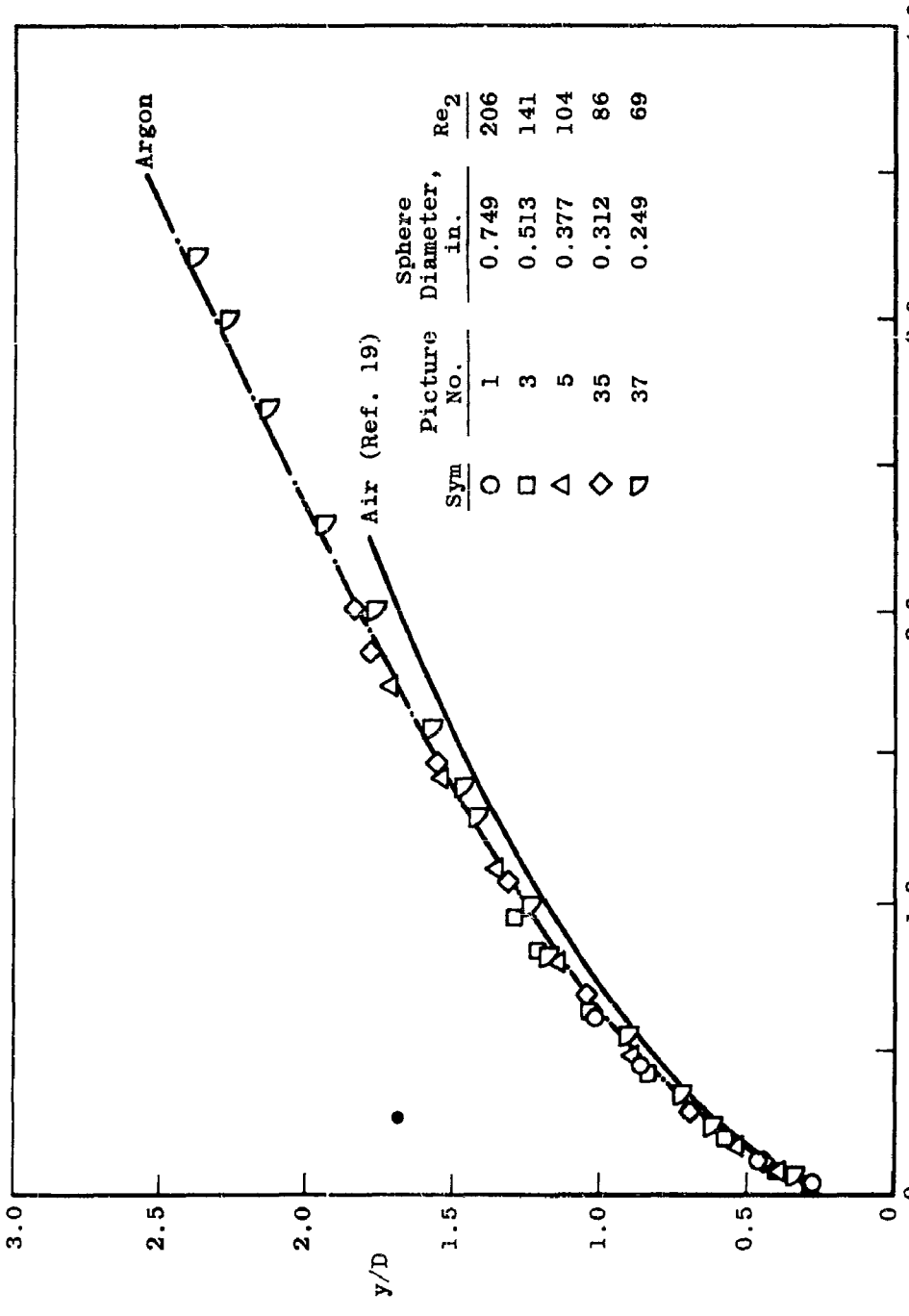

a. M = 4.22, T_o = 2780°K

Fig. 9 Shock Shape for Water-Cooled Sphere

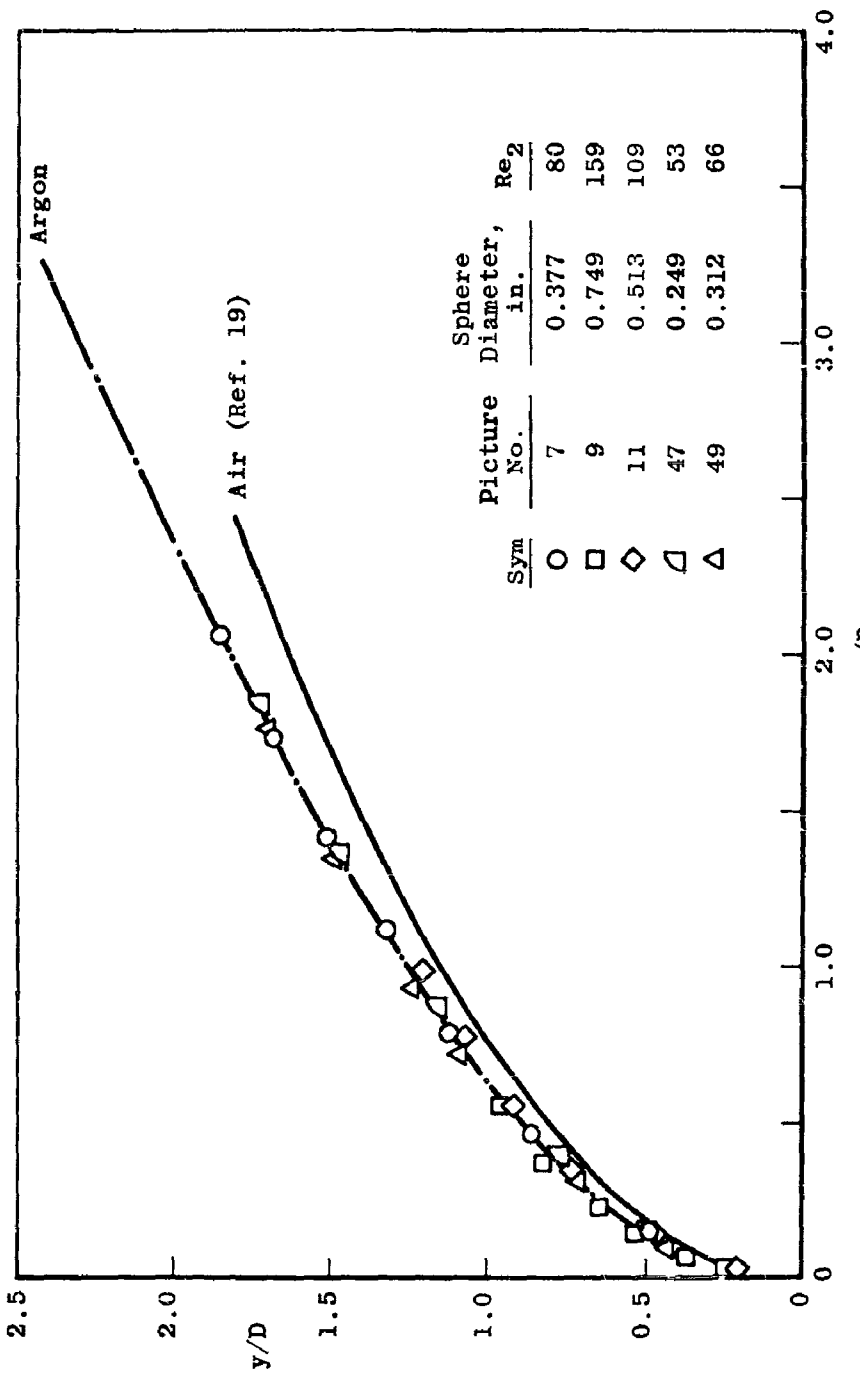

b. M = 4.73, T_o = 2780°K

Fig. 9 Continued

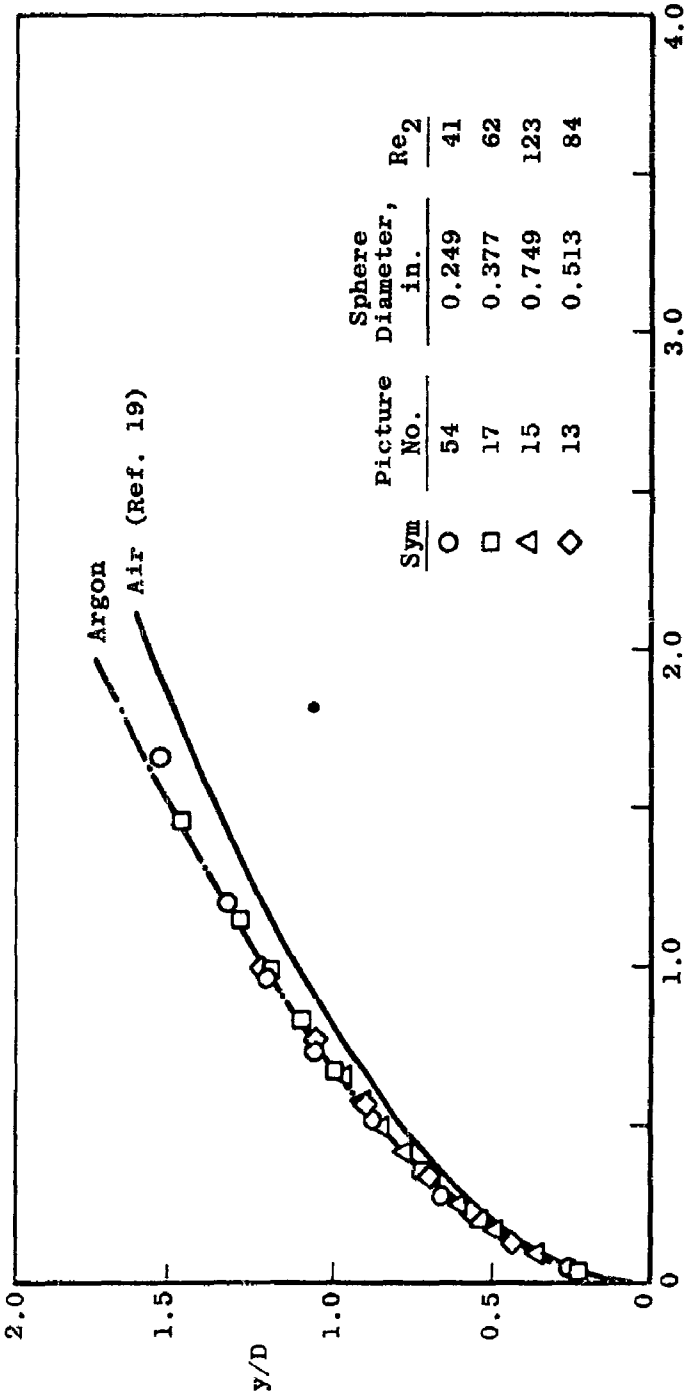

c. M = 5.20, T_o = 2780°K

Fig. 9 Continued

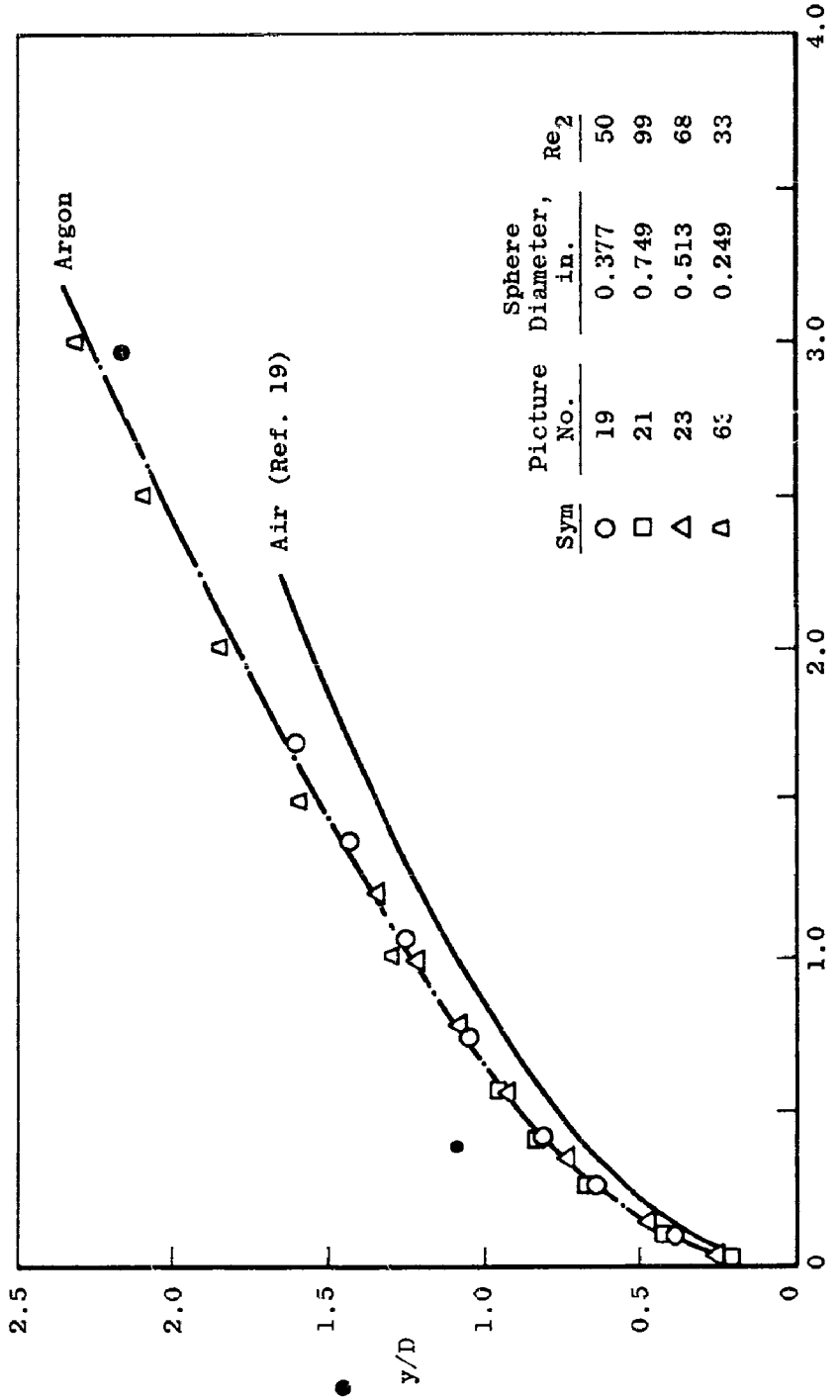

d. M = 5.67, T_o = 2780°K

Fig. 9 Continued

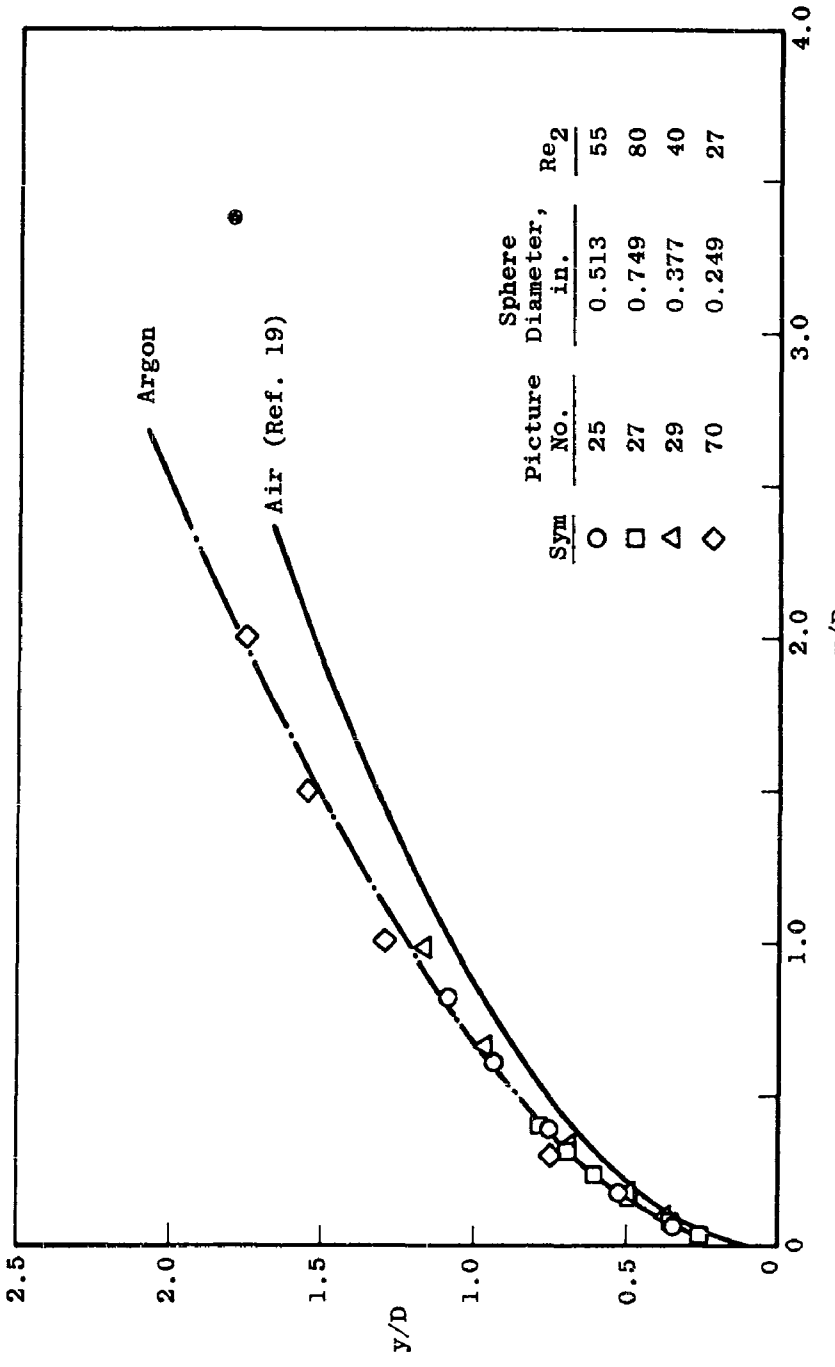

e. M = 6.09, T_o = 2780°K

Fig. 9 Concluded

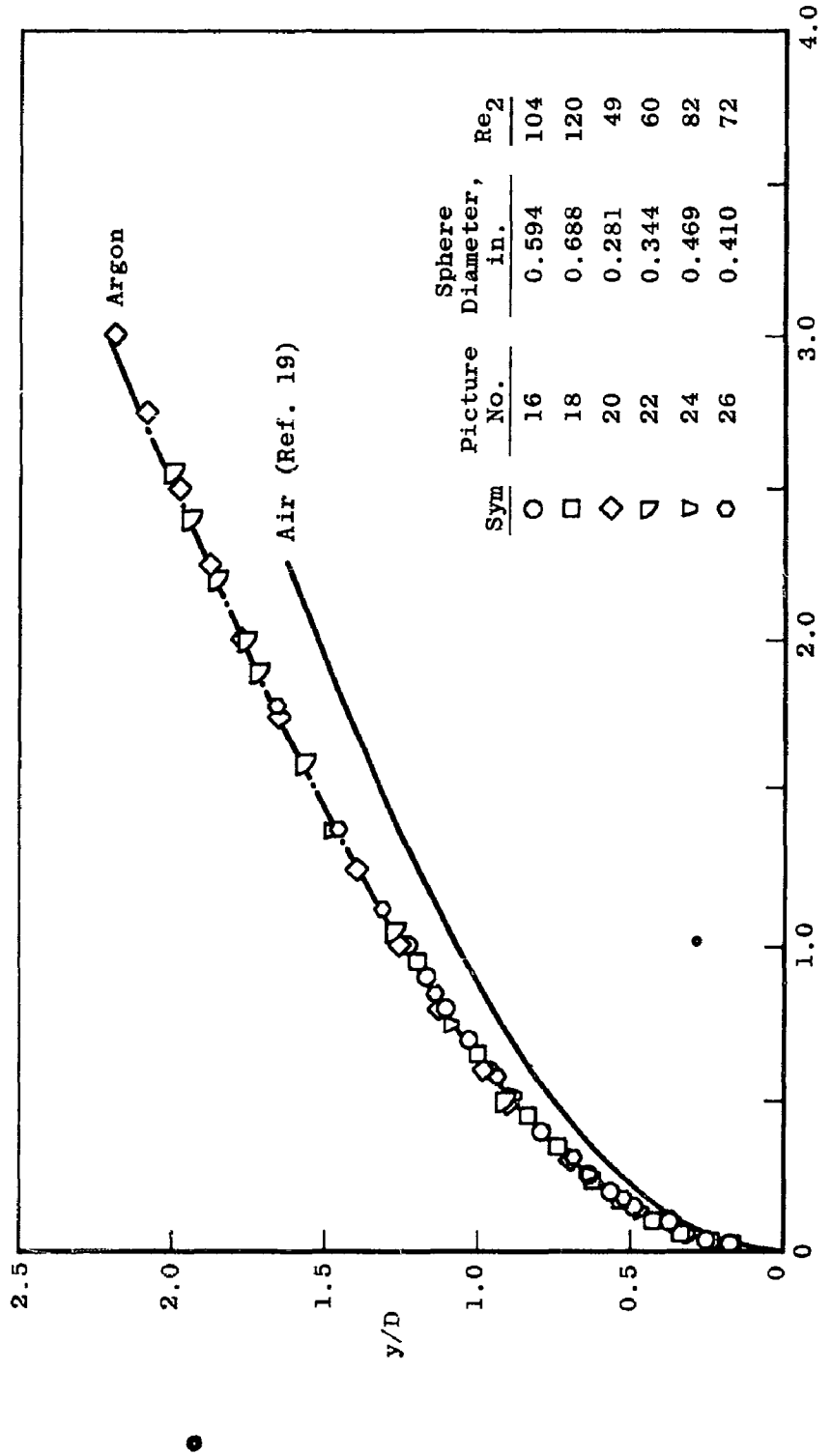

a. M = 6.0, T_o = 3010°K

Fig. 10 Shock Shape for Uncooled Sphere

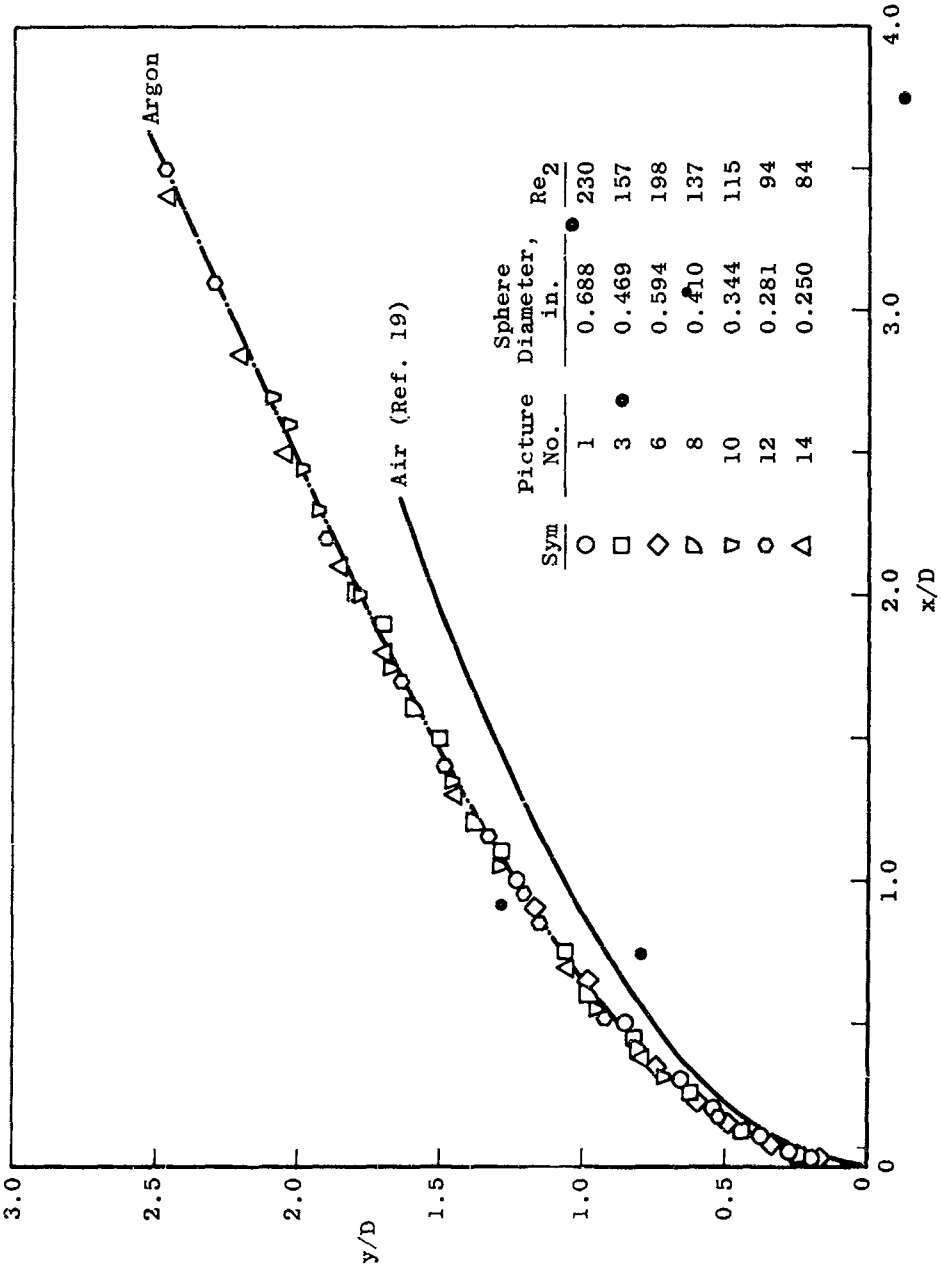

b. M = 6.23, T_o = 2990°K

Fig. 10 Continued

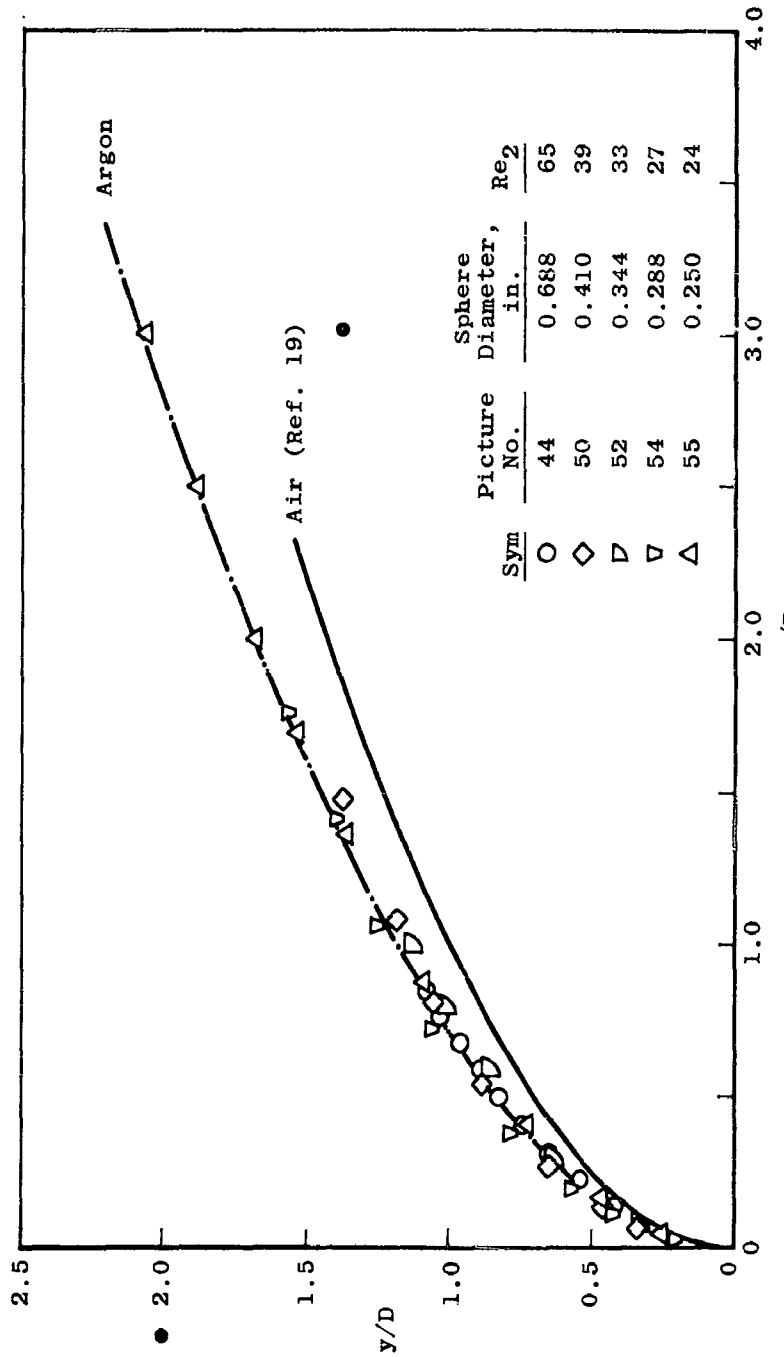

c. M = 8.61, T_o = 4260°K

Fig. 10 Continued

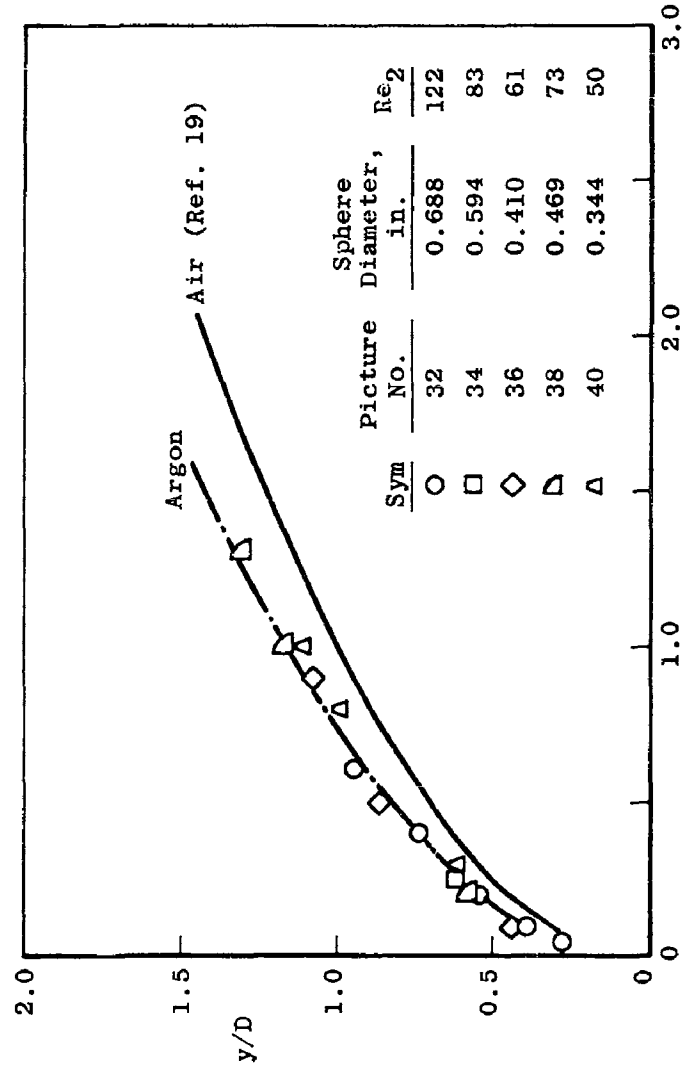

d. M = 9.21, T_o = 3280°K

Fig. 10 Concluded

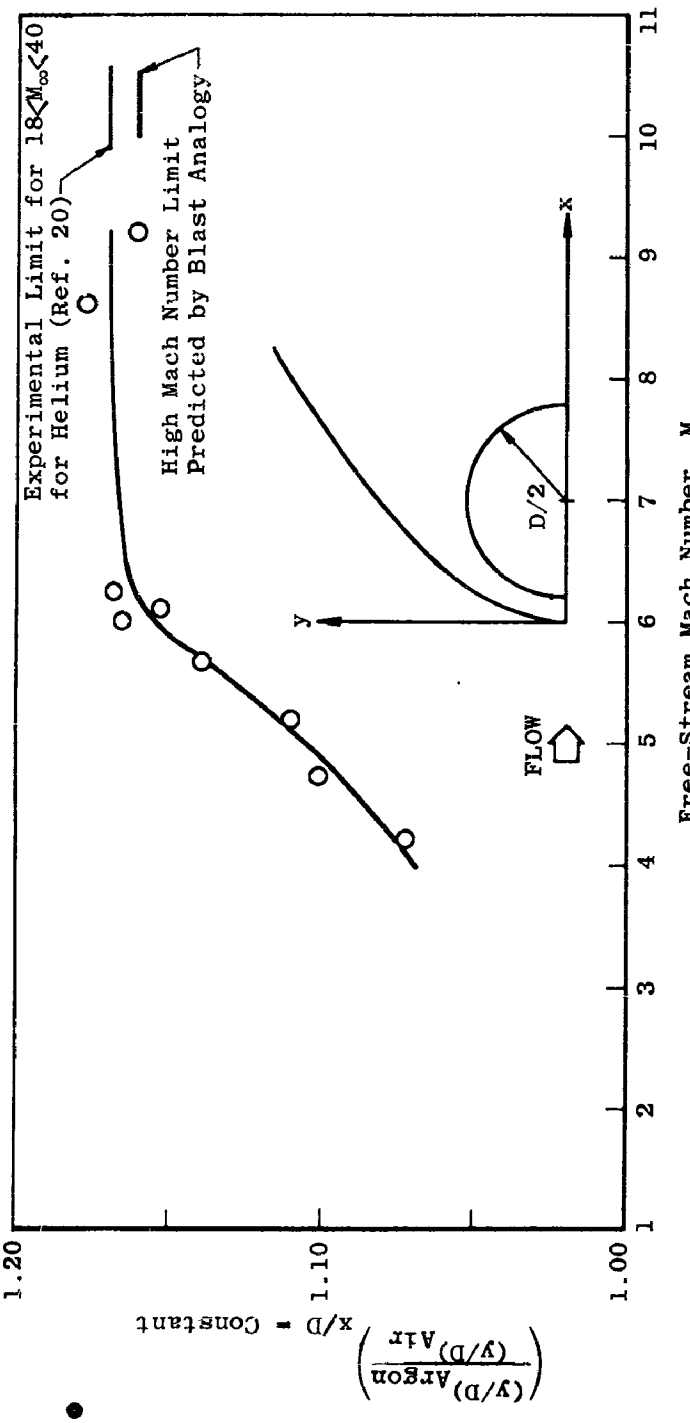

Fig. 11 Comparison of Shock Shapes for Spheres in Argon and Air

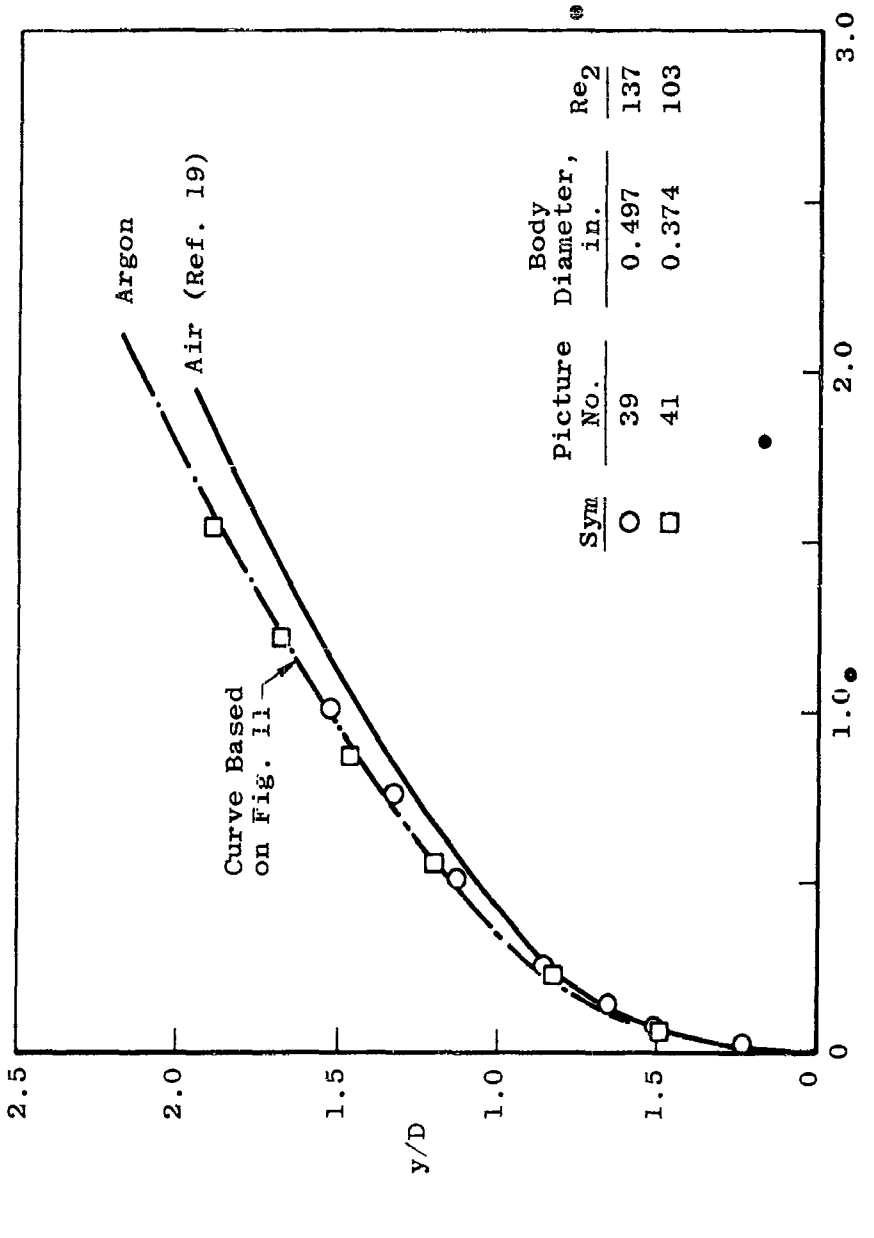

a. M = 4.22, T_o = 2780°K

Fig. 12 Shock Shape for Water-Cooled, Flat-Faced Body

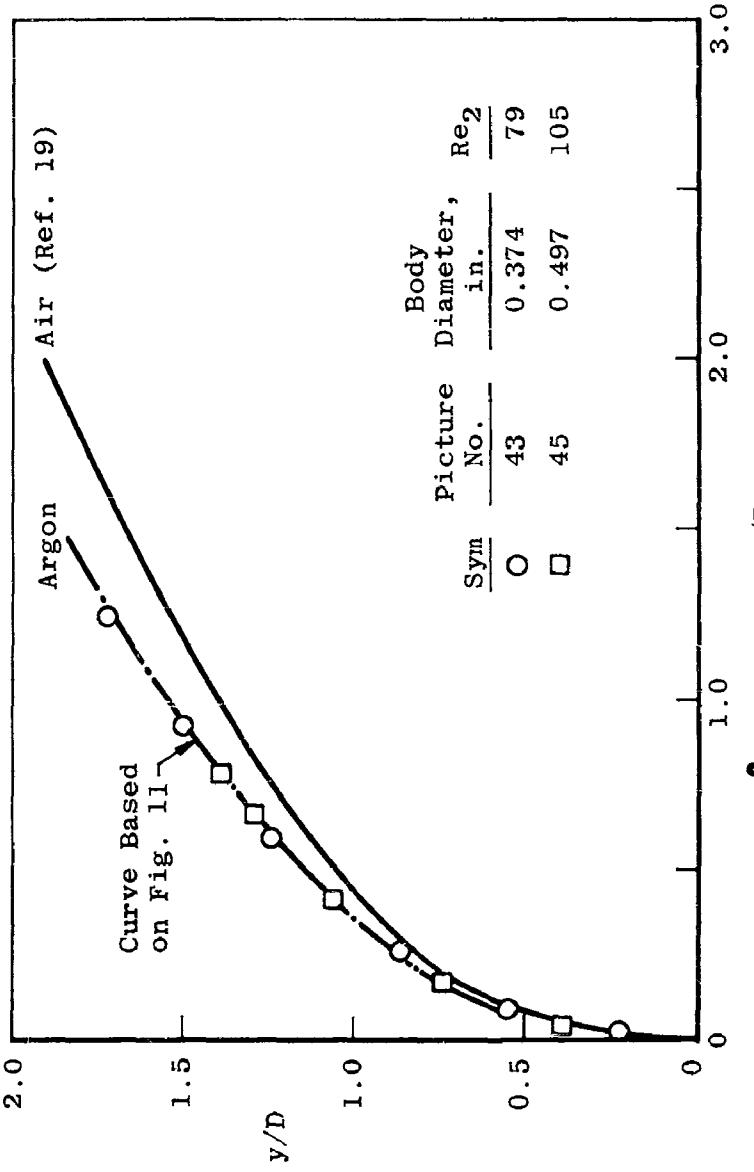

b. M = 4.73, T_o = 2780°K

Fig. 12 Continued

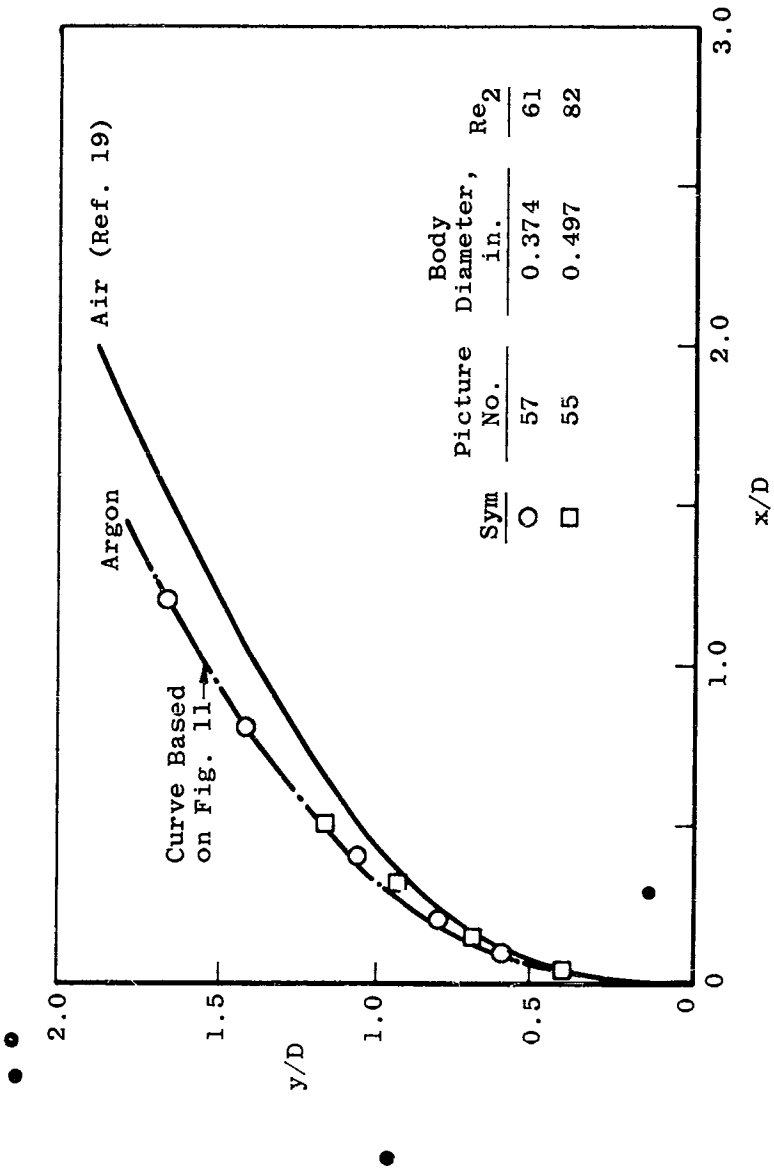

c. M = 5.20, T_o = 2780°K

Fig. 12 Continued

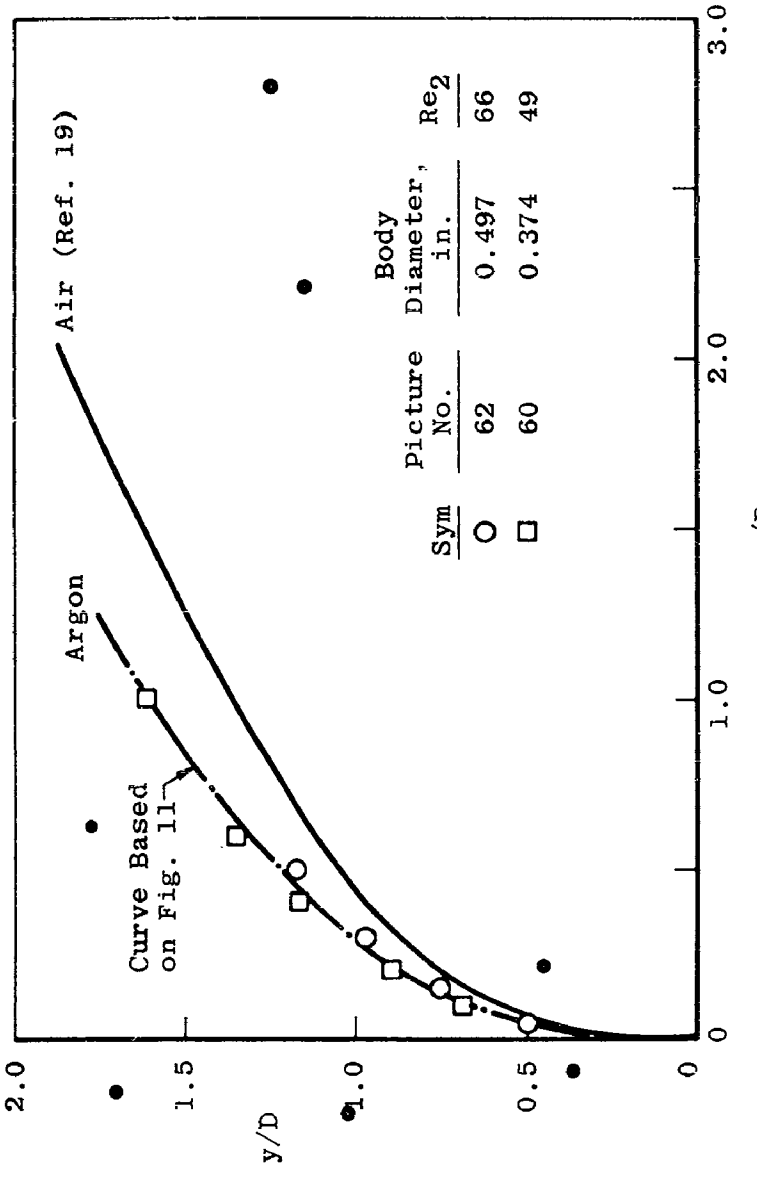

d. M = 5.67, T_o = 2780°K

Fig. 12 Continued

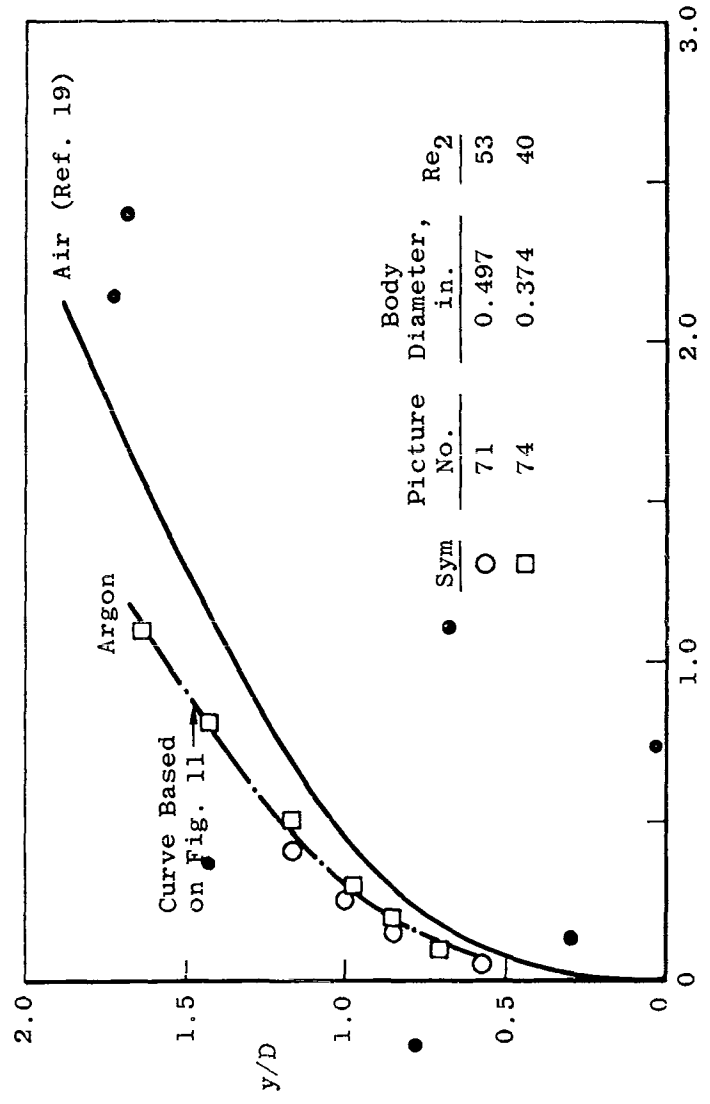

e. M = 6.09, T_o = 2780°K

Fig. 12 Concluded

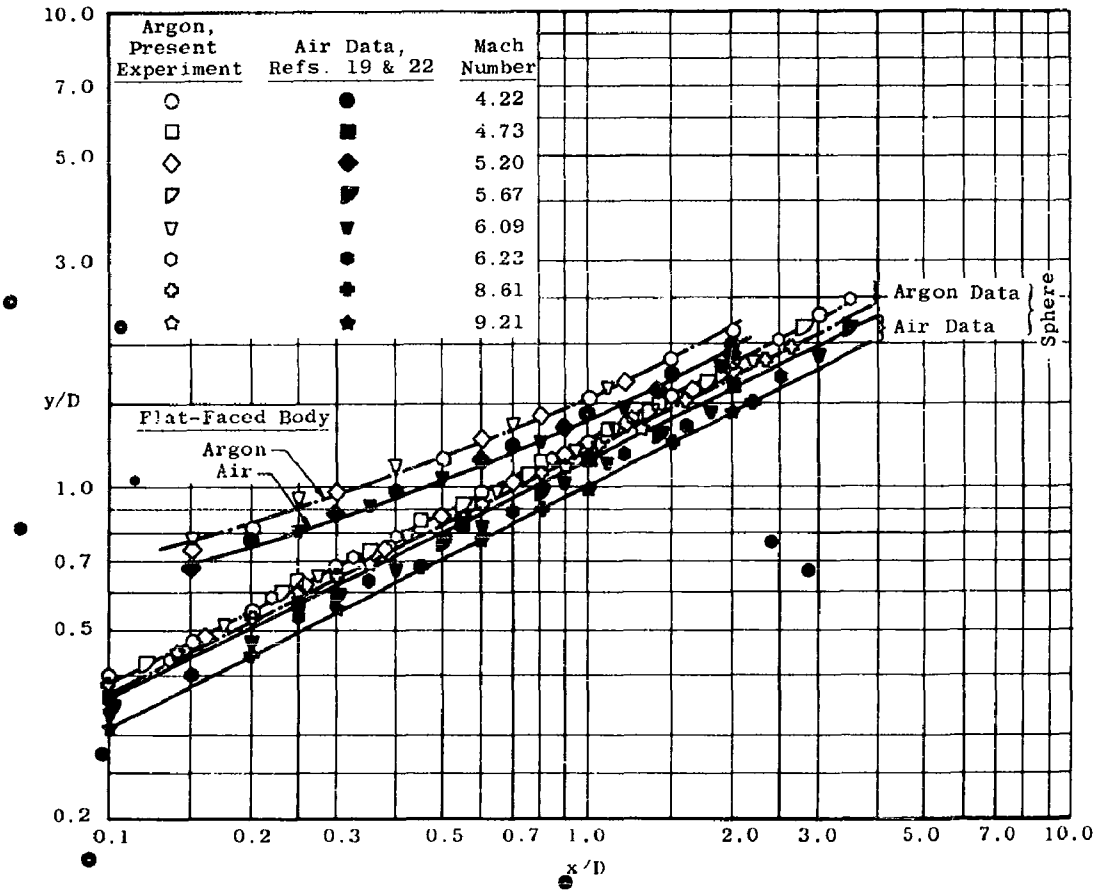

Fig. 13 Correlation of Experimental Shock Shape Data

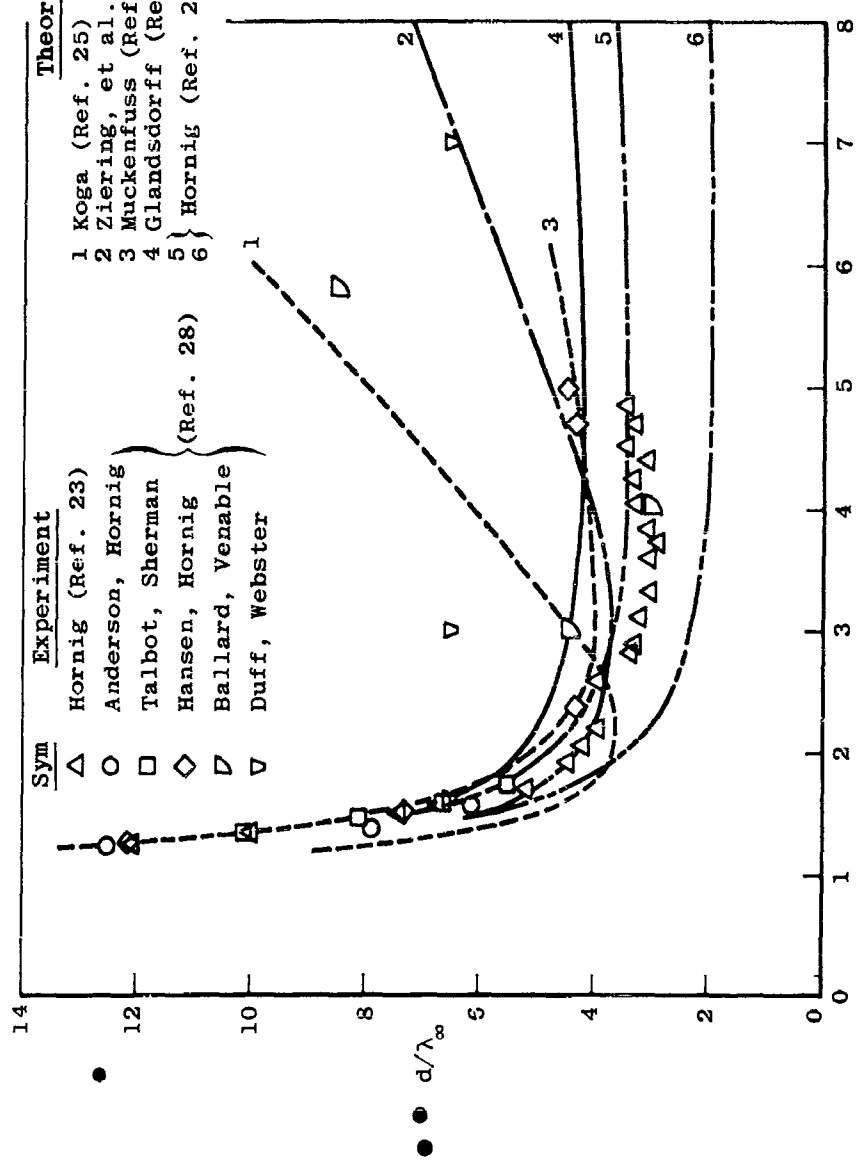

Fig. 14 Variation of Shock-Wave Thickness with Mach Number for Monatomic Gases

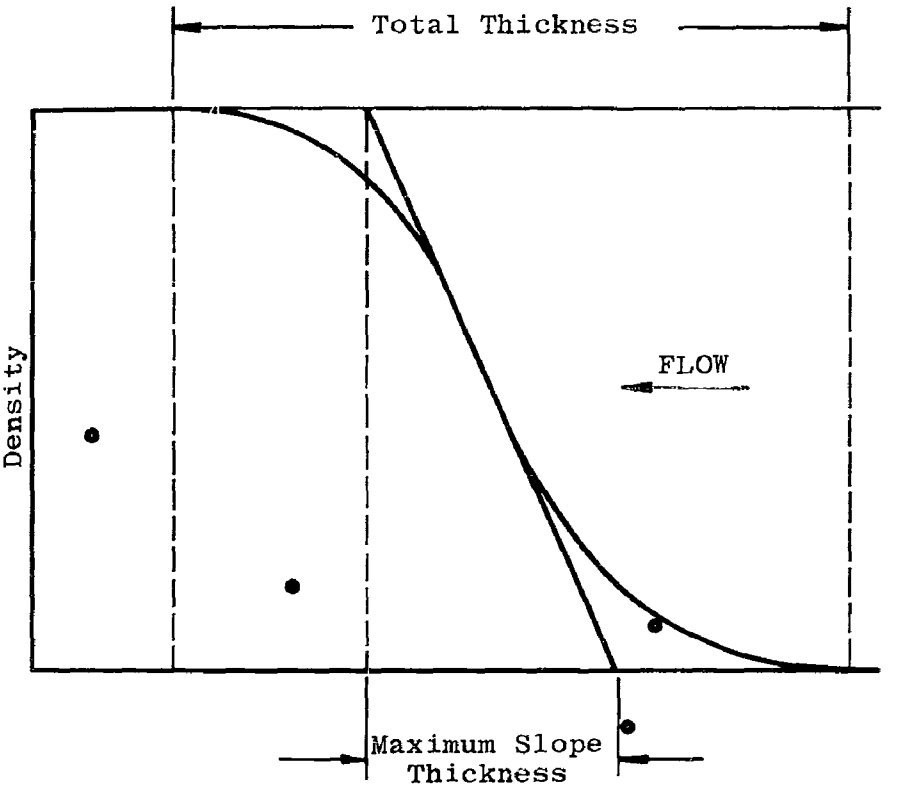

Fig. 15 Shock-Wave Density Profile

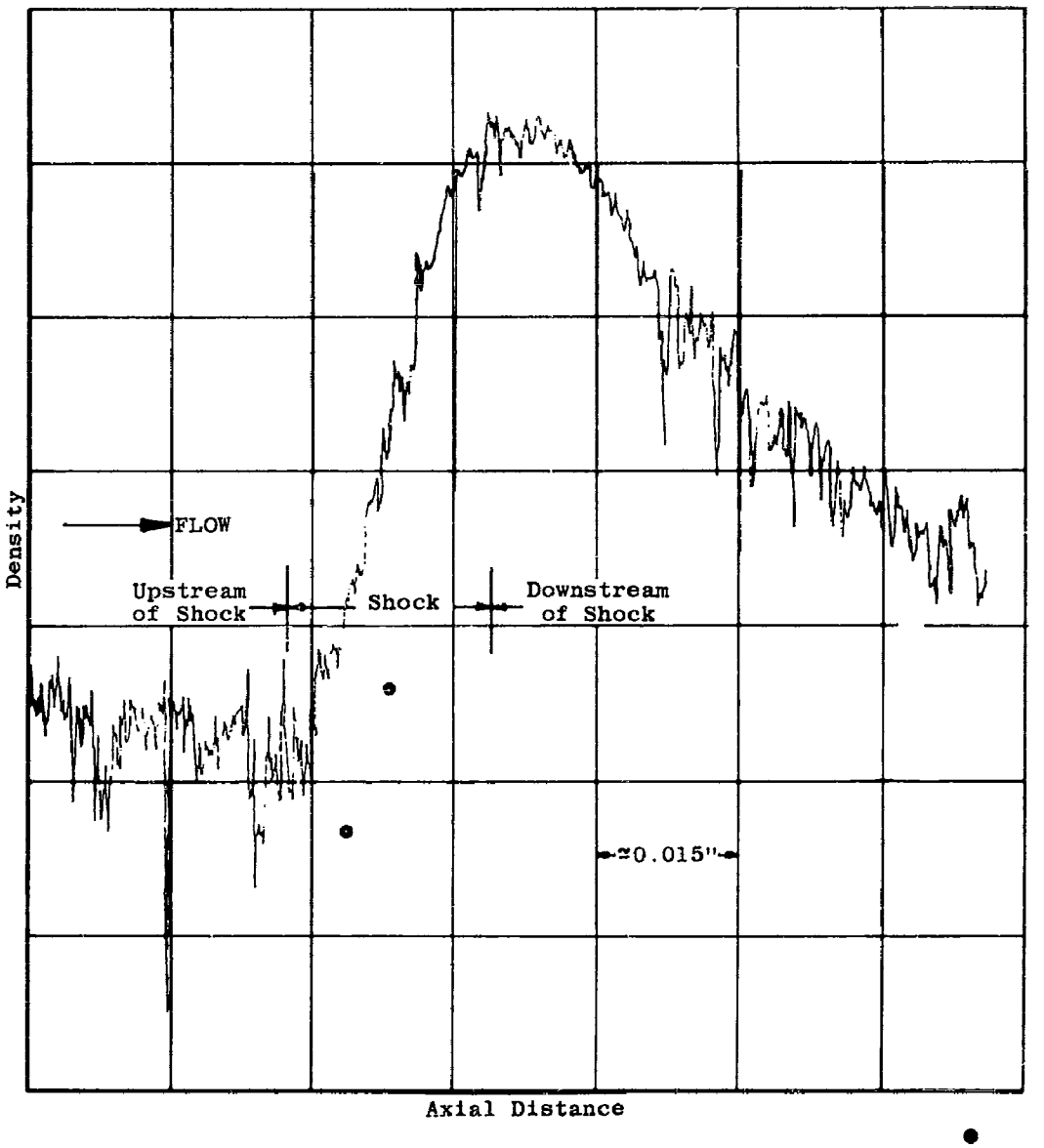

Fig. 16 Typical Film Density Profile through the Shock Wave

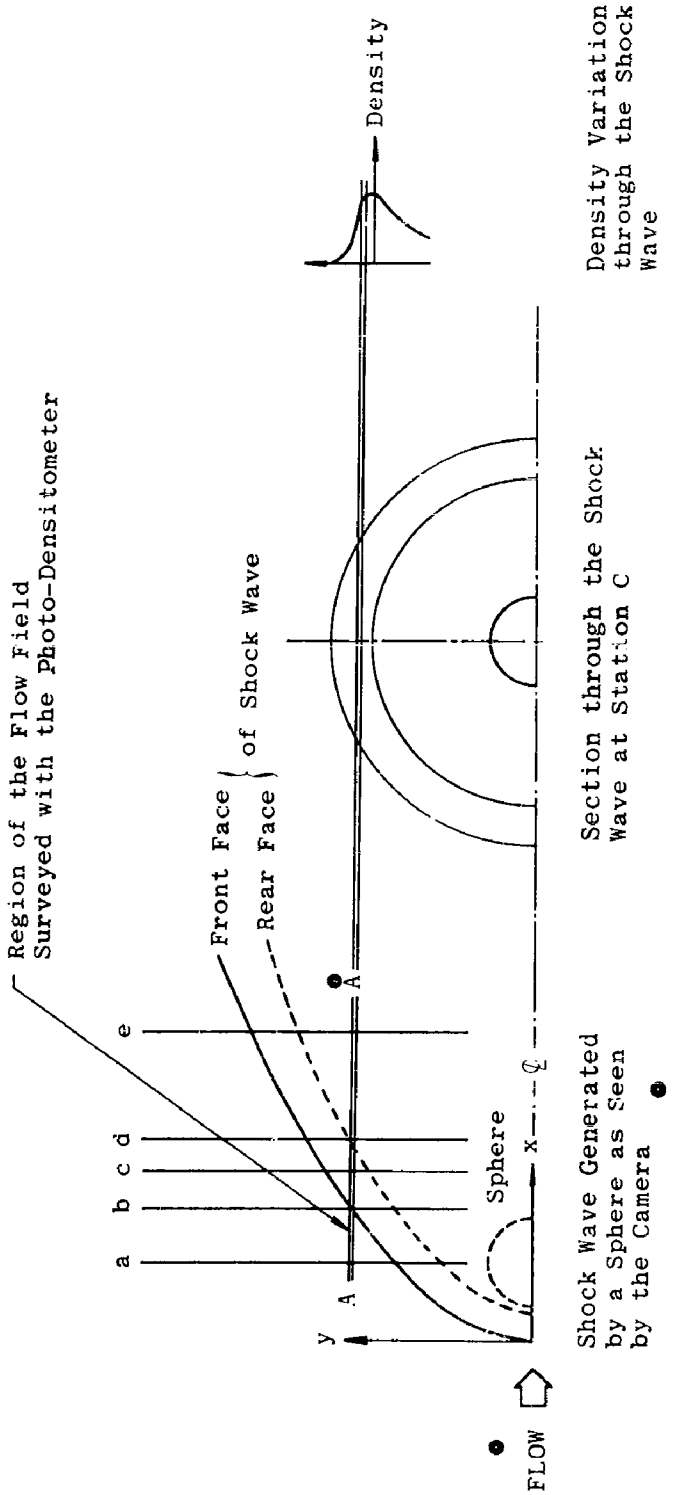

Fig. 17 Three-Dimensional Shock Wave

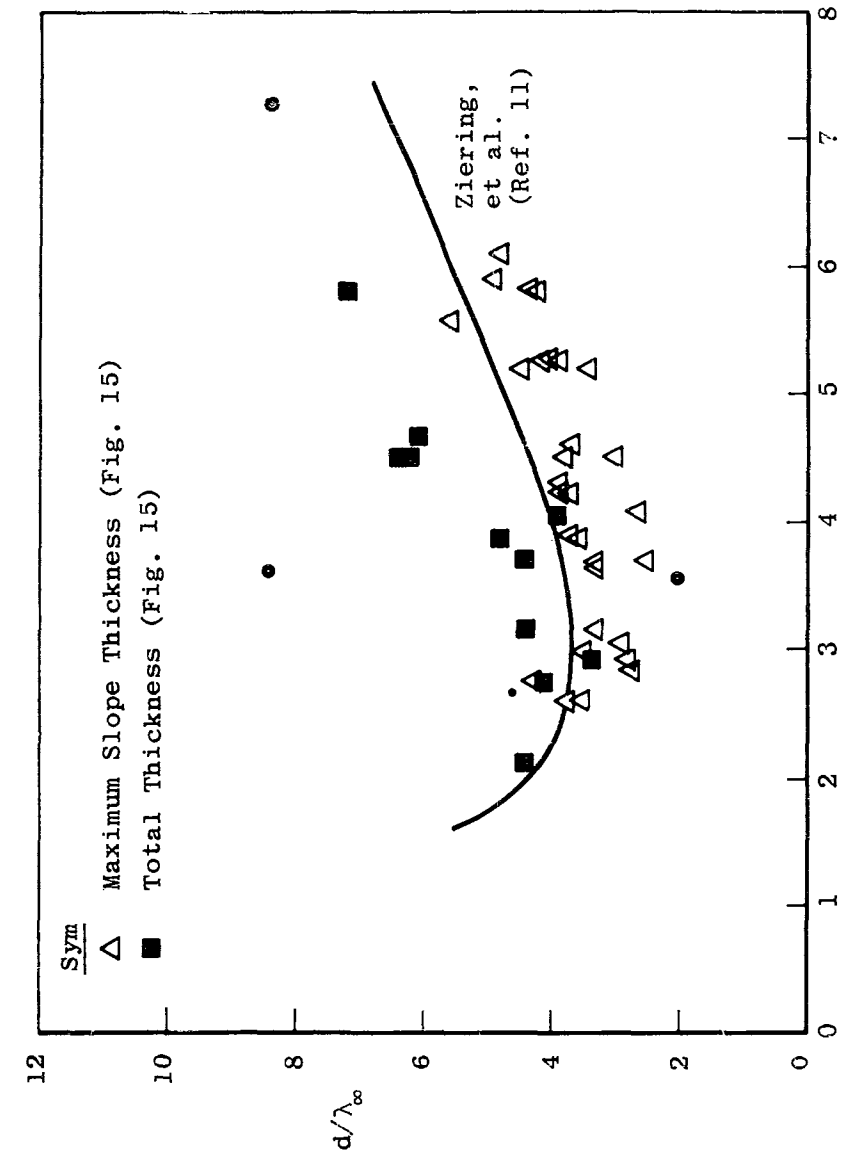

Fig. 18 Experimentally Determined Shock-Wave Thickness in Argon

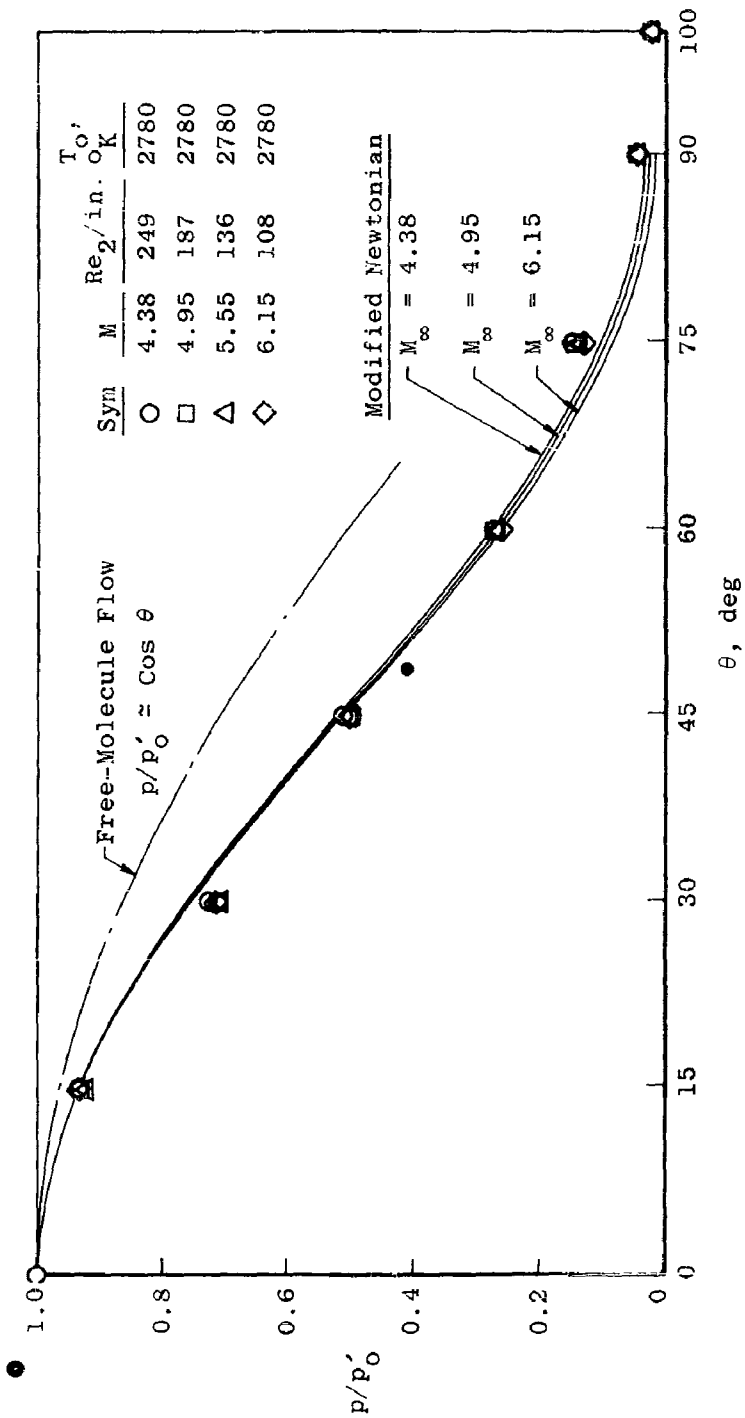

Fig. 19 Surface Pressure Distribution over a Sphere

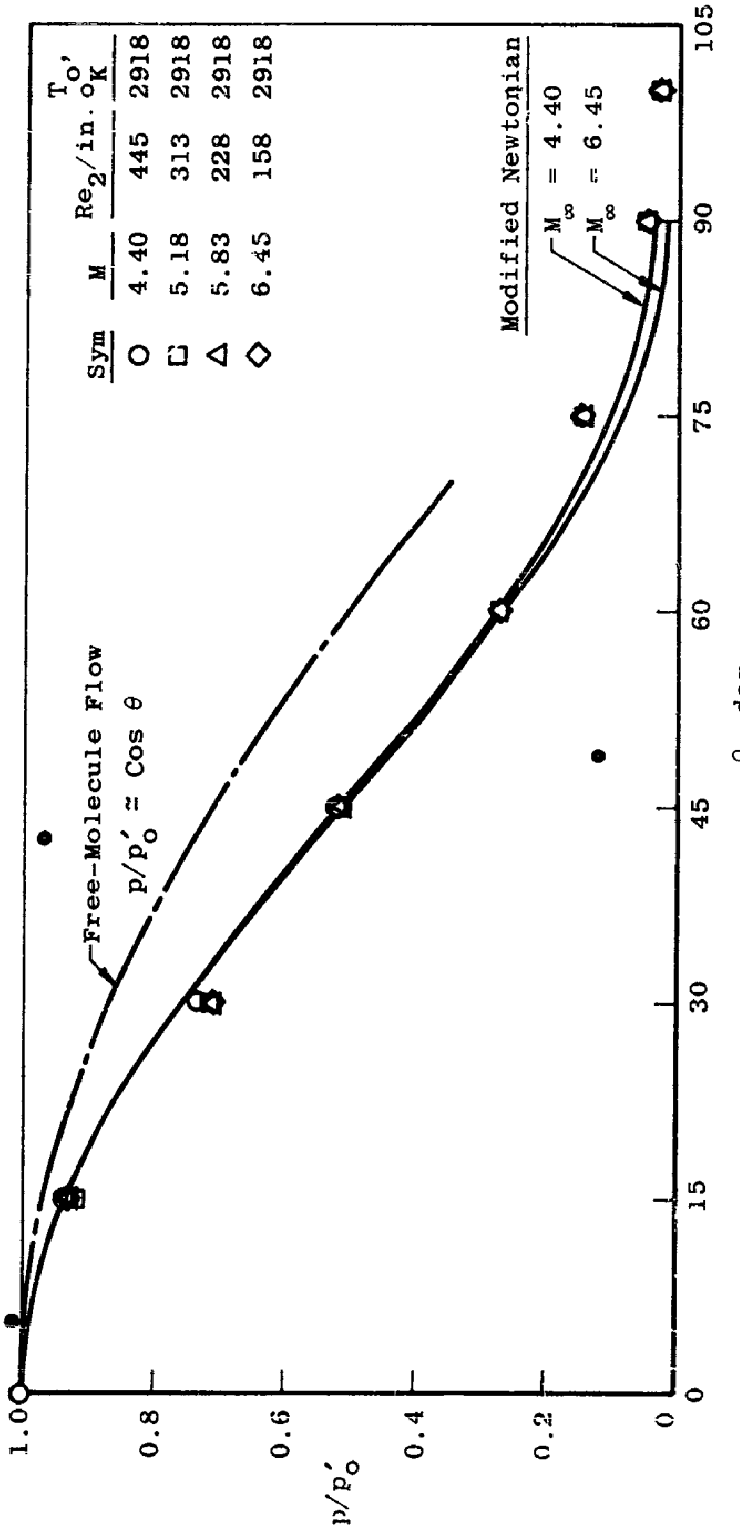

Fig. 19 Continued

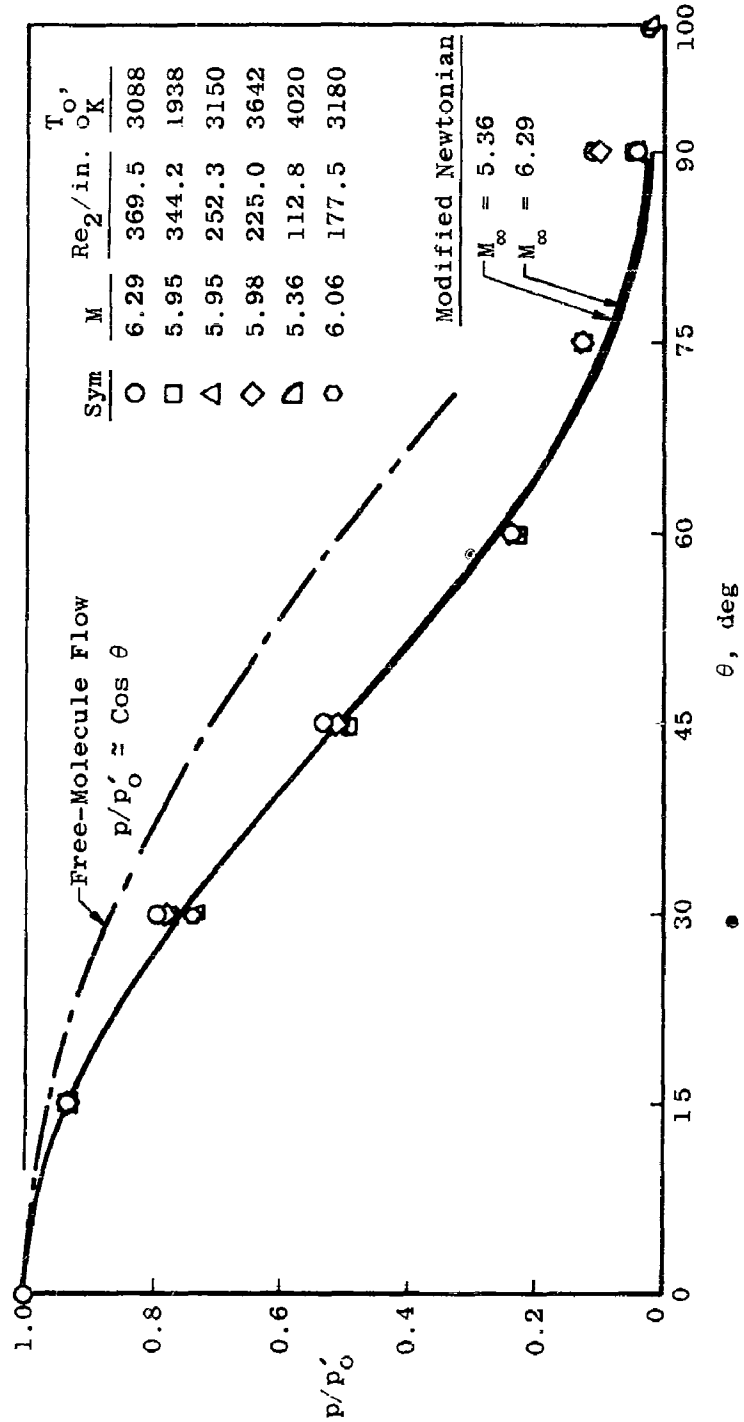

Fig. 19 Continued

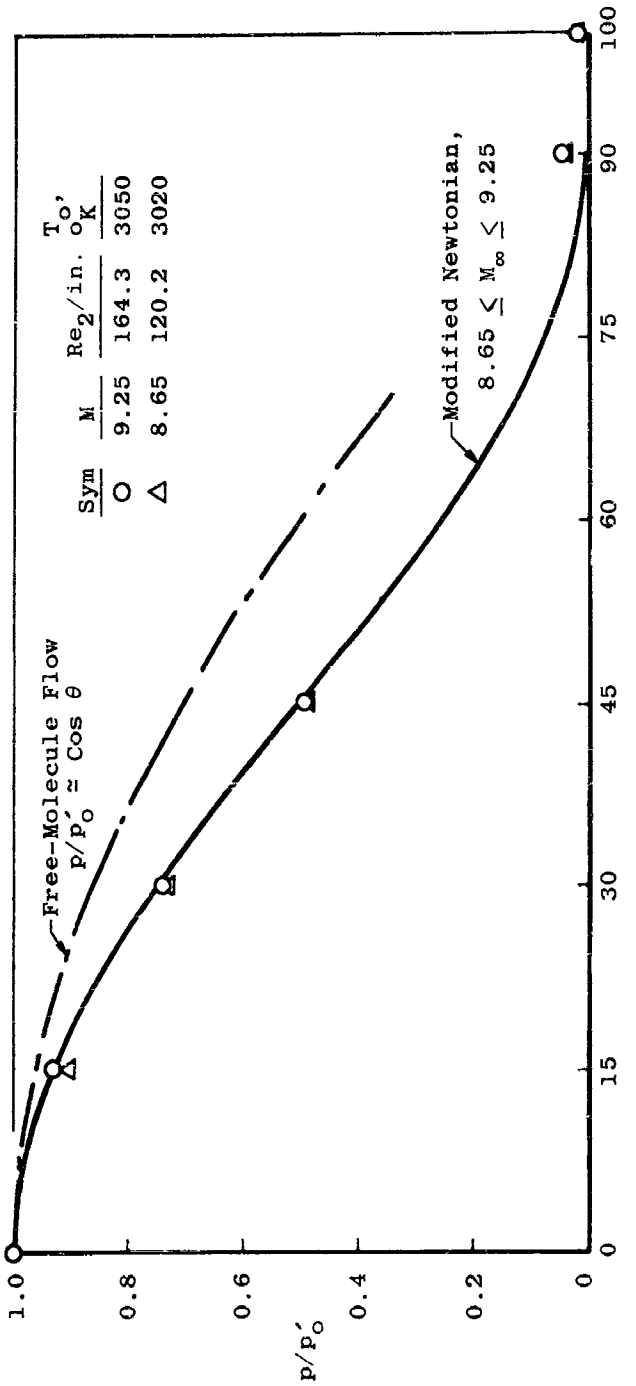

Fig. 19 Continued

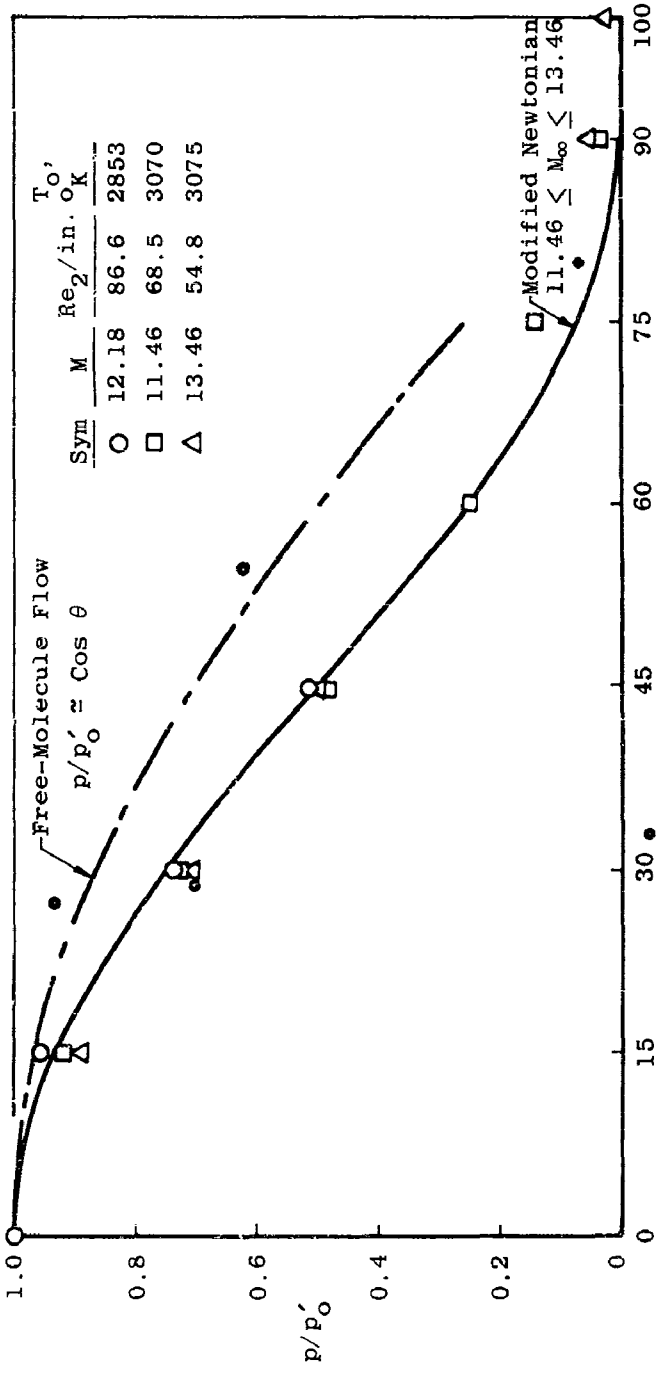

Fig. 19 Concluded

Arnold Engineering Development Center
Arnold Air Force Station, Tennessee
Rpt. No. AEDC-TDR-63-21. THE SHOCK SHAPE AND SHOCK DETACHMENT DISTANCE FOR SPHERES AND FLAT-FACED BODIES IN LOW-DENSITY, HYPERVELOCITY, ARGON FLOW. February 1963. 67 p. incl 32 refs., illus., table.

Unclassified Report

An experimental investigation has been made to determine the pressure distribution, shock shape, and shock detachment distance for spheres and the latter two characteristics for flat-faced bodies in a heated argon flow where M_∞ = 4 to 14, T_o = 1900 to 4100°K, and Re_2 = 25 to 225. The excitation of the argon resulted in a natural flow visualization which enabled photographs of the shocks generated by spheres and flat-faced bodies to be obtained. A photodensitometer was used in the analysis of shock shapes and detachment distances. The blast analogy, and calculations from an empirical relationship proposed by Love were compared with the results of the present investigation. The difference between air and argon was in agreement with that predicted by the blast analogy, i.e., for a constant value of x/D then $(y/D)_{argon}/(y/D)_{air}$ = 1.16. For the lowest Reynolds number tested, the nondimensionalized shock shape is independent of Reynolds number when the effect of Reynolds number on detachment distance is taken into account. The shock detachment distance indicated that the boundary and shock layers were either incipiently or fully merged, and that the detachment distance was a function of wall temperature, Reynolds number, Mach number, and body shape. As the Reynolds number decreases, the shock detachment distance increases to values more than double the "inviscid" values, and for water-cooled bodies the detachment distance decreases to less than the inviscid value before the increase for the lowest Reynolds numbers.

1. Shock waves
2. Spheres
3. Blunt Bodies
4. Hypervelocity flow
5. Argon
I. AFSC Program Area 750A, Project 8953, Task 895306
II. Contract AF 40(600)-1000
III. ARO, Inc., Arnold AF Sta, Tenn.
IV. A. B. Bailey and W. H. Sims
V. Available from OTS
VI. In ASTIA Collection

Arnold Engineering Development Center
Arnold Air Force Station, Tennessee
Rpt. No. AEDC-TDR-63-21. THE SHOCK SHAPE AND SHOCK DETACHMENT DISTANCE FOR SPHERES AND FLAT-FACED BODIES IN LOW-DENSITY, HYPERVELOCITY, ARGON FLOW. February 1963. 67 p. incl 32 refs., illus., table.

Unclassified Report

An experimental investigation has been made to determine the pressure distribution, shock shape, and shock detachment distance for spheres and the latter two characteristics for flat-faced bodies in a heated argon flow where M_∞ = 4 to 14, T_o = 1900 to 4100°K, and Re_2 = 25 to 225. The excitation of the argon resulted in a natural flow visualization which enabled photographs of the shocks generated by spheres and flat-faced bodies to be obtained. A photodensitometer was used in the analysis of shock shapes and detachment distances. The blast analogy, and calculations from an empirical relationship proposed by Love were compared with the results of the present investigation. The difference between air and argon was in agreement with that predicted by the blast analogy, i.e., for a constant value of x/D then $(y/D)_{argon}/(y/D)_{air}$ = 1.16. For the lowest Reynolds number tested, the nondimensionalized shock shape is independent of Reynolds number when the effect of Reynolds number on detachment distance is taken into account. The shock detachment distance indicated that the boundary and shock layers were either incipiently or fully merged, and that the detachment distance was a function of wall temperature, Reynolds number, Mach number, and body shape. As the Reynolds number decreases, the shock detachment distance increases to values more than double the "inviscid" values, and for water-cooled bodies the detachment distance decreases to less than the inviscid value before the increase for the lowest Reynolds numbers.

1. Shock waves
2. Spheres
3. Blunt Bodies
4. Hypervelocity flow
5. Argon
I. AFSC Program Area 750A, Project 8953, Task 895306
II. Contract AF 40(600)-1000
III. ARO, Inc., Arnold AF Sta, Tenn.
IV. A. B. Bailey and W. H. Sims
V. Available from OTS
VI. In ASTIA Collection

Arnold Engineering Development Center
Arnold Air Force Station, Tennessee
Rpt. No. AEDC-TDR-63-21. THE SHOCK SHAPE AND SHOCK DETACHMENT DISTANCE FOR SPHERES AND FLAT-FACED BODIES IN LOW-DENSITY, HYPERVELOCITY, ARGON FLOW. February 1963. 67 p. incl 32 refs., illus., table.

Unclassified Report

An experimental investigation has been made to determine the pressure distribution, shock shape, and shock detachment distance for spheres and the latter two characteristics for flat-faced bodies in a heated argon flow where M_∞ = 4 to 14, T_0 = 1900 to 4100°K, and Re_2 = 25 to 725. The excitation of the argon resulted in a natural flow visualization which enabled photographs of the shocks generated by spheres and flat-faced bodies to be obtained. A photodensitometer was used in the analysis of shock shapes and detachment distances. The blast analogy, and calculations from an empirical relationship proposed by Love were compared with the results of the present investigation. The difference between air and argon was in agreement with that predicted by the blast analogy, i.e., for a constant value of x/D then $(y/D)_{argon}/(y/D)_{air}$ = 1.16. For the lowest Reynolds number tested, the nondimensionalized shock shape is independent of Reynolds number when the effect of Reynolds number on detachment distance is taken into account. The shock detachment distance indicated that the boundary and shock layers were either incipiently or fully merged, and that the detachment distance was a function of wall temperature, Reynolds number, Mach number, and body shape. As the Reynolds number decreases, the shock detachment distance increases to values more than double the "inviscid" values, and for water-cooled bodies the detachment distance decreases to less than the inviscid value before the increase for the lowest Reynolds numbers.

1. Shock waves
2. Spheres
3. Blunt Bodies
4. Hypervelocity flow
5. Argon
I. AFSC Program Area 750A, Project 8953, Task 895306
II. Contract AF 40(600)-1000
III. ARO, Inc., Arnold AF Sta, Tenn.
IV. A. B. Bailey and W. H. Sims
V. Available from OTS
VI. In ASTIA Collection

Arnold Engineering Development Center
Arnold Air Force Station, Tennessee
Rpt. No. AEDC-TDR-63-21. THE SHOCK SHAPE AND SHOCK DETACHMENT DISTANCE FOR SPHERES AND FLAT-FACED BODIES IN LOW-DENSITY, HYPERVELOCITY, ARGON FLOW. February 1963. 67 p. incl 32 refs., illus., table.

Unclassified Report

An experimental investigation has been made to determine the pressure distribution, shock shape, and shock detachment distance for spheres and the latter two characteristics for flat-faced bodies in a heated argon flow where M_∞ = 4 to 14, T_0 = 1900 to 4100°K, and Re_2 = 25 to 225. The excitation of the argon resulted in a natural flow visualization which enabled photographs of the shocks generated by spheres and flat-faced bodies to be obtained. A photodensitometer was used in the analysis of shock shapes and detachment distances. The blast analogy, and calculations from an empirical relationship proposed by Love were compared with the results of the present investigation. The difference between air and argon was in agreement with that predicted by the blast analogy, i.e., for a constant value of x/D then $(y/D)_{argon}/(y/D)_{air}$ = 1.16. For the lowest Reynolds number tested, the nondimensionalized shock shape is independent of Reynolds number when the effect of Reynolds number on detachment distance is taken into account. The shock detachment distance indicated that the boundary and shock layers were either incipiently or fully merged, and that the detachment distance was a function of wall temperature, Reynolds number, Mach number, and body shape. As the Reynolds number decreases, the shock detachment distance increases to values more than double the "inviscid" values, and for water-cooled bodies the detachment distance decreases to less than the inviscid value before the increase for the lowest Reynolds numbers.

1. Shock waves
2. Spheres
3. Blunt Bodies
4. Hypervelocity flow
5. Argon
I. AFSC Program Area 750A, Project 8953, Task 895306
II. Contract AF 40(600)-1000
III. ARO, Inc., Arnold AF Sta, Tenn.
IV. A. B. Bailey and W. H. Sims
V. Available from OTS
VI. In ASTIA Collection

Arnold Engineering Development Center
Arnold Air Force Station, Tennessee
Rpt. No. AEDC-TDR-63-21. THE SHOCK SHAPE AND SHOCK DETACHMENT DISTANCE FOR SPHERES AND FLAT-FACED BODIES IN LOW-DENSITY, HYPERVELOCITY, ARGON FLOW. February 1963. 67 p. incl 32 refs., illus., table.

Unclassified Report

An experimental investigation has been made to determine the pressure distribution, shock shape, and shock detachment distance for spheres and the latter two characteristics for flat-faced bodies in a heated argon flow where M_∞ = 4 to 14, T_0 = 1900 to 4100°K, and Re_2 = 25 to 225. The excitation of the argon resulted in a natural flow visualization which enabled photographs of the shocks generated by spheres and flat-faced bodies to be obtained. A photodensitometer was used in the analysis of shock shapes and detachment distances. The blast analogy, and calculations from an empirical relationship proposed by Love were compared with the results of the present investigation. The difference between air and argon was in agreement with that predicted by the blast analogy, i.e., for a constant value of x/D then $(y/D)_{argon}/(y/D)_{air}$ = 1.16. For the lowest Reynolds number tested, the nondimensionalized shock shape is independent of Reynolds number when the effect of Reynolds number on detachment distance is taken into account. The shock detachment distance indicated that the boundary and shock layers were either incipiently or fully merged, and that the detachment distance was a function of wall temperature, Reynolds number, Mach number, and body shape. As the Reynolds number decreases, the shock detachment distance increases to values more than double the "inviscid" values, and for water-cooled bodies the detachment distance decreases to less than the inviscid value before the increase for the lowest Reynolds numbers.

1. Shock waves
2. Spheres
3. Blunt Bodies
4. Hypervelocity flow
5. Argon
I. AFSC Program Area 750A, Project 8953, Task 895306
II. Contract AF 40(600)-1000
III. ARO, Inc., Arnold AF Sta, Tenn.
IV. A. B. Bailey and W. H. Sims
V. Available from OTS
VI. In ASTIA Collection

Arnold Engineering Development Center
Arnold Air Force Station, Tennessee
Rpt. No. AEDC-TDR-63-21. THE SHOCK SHAPE AND SHOCK DETACHMENT DISTANCE FOR SPHERES AND FLAT-FACED BODIES IN LOW-DENSITY, HYPERVELOCITY, ARGON FLOW. February 1963. 67 p. incl 32 refs., illus., table.

Unclassified Report

An experimental investigation has been made to determine the pressure distribution, shock shape, and shock detachment distance for spheres and the latter two characteristics for flat-faced bodies in a heated argon flow where M_∞ = 4 to 14, T_0 = 1900 to 4100°K, and Re_2 = 25 to 225. The excitation of the argon resulted in a natural flow visualization which enabled photographs of the shocks generated by spheres and flat-faced bodies to be obtained. A photodensitometer was used in the analysis of shock shapes and detachment distances. The blast analogy, and calculations from an empirical relationship proposed by Love were compared with the results of the present investigation. The difference between air and argon was in agreement with that predicted by the blast analogy, i.e., for a constant value of x/D then $(y/D)_{argon}/(y/D)_{air}$ = 1.16. For the lowest Reynolds number tested, the nondimensionalized shock shape is independent of Reynolds number when the effect of Reynolds number on detachment distance is taken into account. The shock detachment distance indicated that the boundary and shock layers were either incipiently or fully merged, and that the detachment distance was a function of wall temperature, Reynolds number, Mach number, and body shape. As the Reynolds number decreases, the shock detachment distance increases to values more than double the "inviscid" values, and for water-cooled bodies the detachment distance decreases to less than the inviscid value before the increase for the lowest Reynolds numbers.

1. Shock waves
2. Spheres
3. Blunt Bodies
4. Hypervelocity flow
5. Argon
I. AFSC Program Area 750A, Project 8953, Task 895306
II. Contract AF 40(600)-1000
III. ARO, Inc., Arnold AF Sta, Tenn.
IV. A. B. Bailey and W. H. Sims
V. Available from OTS
VI. In ASTIA Collection

Arnold Engineering Development Center
Arnold Air Force Station, Tennessee
Rpt. No. AEDC-TDR-63-21. THE SHOCK SHAPE AND SHOCK DETACHMENT DISTANCE FOR SPHERES AND FLAT-FACED BODIES IN LOW-DENSITY, HYPERVELOCITY, ARGON FLOW. February 1963. 67 p. incl 32 refs., illus., table.

Unclassified Report

An experimental investigation has been made to determine the pressure distribution, shock shape, and shock detachment distance for spheres and the latter two characteristics for flat-faced bodies in a heated argon flow where M_∞ = 4 to 14, T_o = 1900 to 4100°K, and Re_2 = 25 to 225. The excitation of the argon resulted in a natural flow visualization which enabled photographs of the shocks generated by spheres and flat-faced bodies to be obtained. A photodensitometer was used in the analysis of shock shapes and detachment distances. The blast analogy, and calculations from an empirical relationship proposed by Love were compared with the results of the present investigation. The difference between air and argon was in agreement with that predicted by the blast analogy, i.e., for a constant value of x/D then $(y/D)_{argon}/(y/D)_{air}$ = 1.16. For the lowest Reynolds number tested, the nondimensionalized shock shape is independent of Reynolds number when the effect of Reynolds number on detachment distance is taken into account. The shock detachment distance indicated that the boundary and shock layers were either incipiently or fully merged, and that the detachment distance was a function of wall temperature, Reynolds number, Mach number, and body shape. As the Reynolds number decreases, the shock detachment distance increases to values more than double the "inviscid" values, and for water-cooled bodies the detachment distance decreases to less than the inviscid value before the increase for the lowest Reynolds numbers.

1. Shock waves
2. Spheres
3. Blunt Bodies
4. Hypervelocity flow
5. Argon
I. AFSC Program Area 750A, Project 8953, Task 895306
II. Contract AF 40(600)-1000
III. ARO, Inc., Arnold AF Sta, Tenn.
IV. A. B. Bailey and W. H. Sims
V. Available from OTS
VI. In ASTIA Collection

Arnold Engineering Development Center
Arnold Air Force Station, Tennessee
Rpt. No. AEDC-TDR-63-21. THE SHOCK SHAPE AND SHOCK DETACHMENT DISTANCE FOR SPHERES AND FLAT-FACED BODIES IN LOW-DENSITY, HYPERVELOCITY, ARGON FLOW. February 1963. 67 p. incl 32 refs., illus., table.

Unclassified Report

An experimental investigation has been made to determine the pressure distribution, shock shape, and shock detachment distance for spheres and the latter two characteristics for flat-faced bodies in a heated argon flow where M_∞ = 4 to 14, T_o = 1900 to 4100°K, and Re_2 = 25 to 225. The excitation of the argon resulted in a natural flow visualization which enabled photographs of the shocks generated by spheres and flat-faced bodies to be obtained. A photodensitometer was used in the analysis of shock shapes and detachment distances. The blast analogy, and calculations from an empirical relationship proposed by Love were compared with the results of the present investigation. The difference between air and argon was in agreement with that predicted by the blast analogy, i.e., for a constant value of x/D then $(y/D)_{argon}/(y/D)_{air}$ = 1.16. For the lowest Reynolds number tested, the nondimensionalized shock shape is independent of Reynolds number when the effect of Reynolds number on detachment distance is taken into account. The shock detachment distance indicated that the boundary and shock layers were either incipiently or fully merged, and that the detachment distance was a function of wall temperature, Reynolds number, Mach number, and body shape. As the Reynolds number decreases, the shock detachment distance increases to values more than double the "inviscid" values, and for water-cooled bodies the detachment distance decreases to less than the inviscid value before the increase for the lowest Reynolds numbers.

1. Shock waves
2. Spheres
3. Blunt Bodies
4. Hypervelocity flow
5. Argon
I. AFSC Program Area 750A, Project 8953, Task 895306
II. Contract AF 40(600)-1000
III. ARO, Inc., Arnold AF Sta, Tenn.
IV. A. B. Bailey and W. H. Sims
V. Available from OTS
VI. In ASTIA Collection

UNCLASSIFIED